HAW HAMBURG

Bachelor thesis

Nataliya Didukh, Ihor Zhvanko

Human joint angle measurement exploiting kinematic constraints using an inertial motion capture system

Fakultät Technik und Informatik
Department Informatik

Faculty of Computer Science and Engineering
Department Computer Science

Nataliya Didukh, Ihor Zhvanko

Human joint angle measurement exploiting kinematic constraints using an inertial motion capture system

Bachelorarbeit eingereicht im Rahmen der Bachelorprüfung
im Studiengang *Bachelor of Science Informatik Technischer Systeme*
am Department Informatik
der Fakultät Technik und Informatik
der Hochschule für Angewandte Wissenschaften Hamburg

Betreuender Prüfer: Prof. Dr. Kai von Luck
Zweitgutachter: Dr. Jan Schwarzer

Eingereicht am: February 5, 2023

Nataliya Didukh, Ihor Zhvanko

Thema der Arbeit

Messung menschlicher Gelenkwinkel unter Ausnutzung kinematischer Randbedingungen mithilfe eines inertialen Motion-Capture-Systems.

Stichworte

IMU, Gelenk, Winkel, Scharnier, ART (Tracking-System), optische Erfassung, inertiale Erfassung, kinematische Randbedingungen, Optimierung, Partikelfilter

Kurzzusammenfassung

Die genaue Messung menschlicher Gelenkwinkel ist in der Biomechanik entscheidend und wirkt sich auf Bereiche wie Sportwissenschaft und Rehabilitation aus. Diese Arbeit stellt eine Kalibrationsmethode für die Messung von Gelenkwinkeln mit einem inertialen Motion-Capture-System unter Verwendung von Partikelfiltermethoden vor, mit dem Ziel, die Genauigkeit der Echtzeitwinkelmessung zu verbessern.

Die Methodik verwendet sequentielles Importance Sampling, um die Beugungs-/Streckungsachsen des Kniegelenks mithilfe von zwei Inertial Measurement Units (IMUs) zu bestimmen. Die beste Schätzung des Kniegelenks wird dann verwendet, um den Beugungs-/Streckungswinkel des Knies zu messen. Die Ergebnisse zeigen eine bemerkenswerte etwa 4° RMSE im Vergleich zur optischen Erfassung, wobei der Algorithmus sich als stabil bei unterschiedlichen Sensorplatzierungen und Übungen erweist.

Die Beiträge umfassen die Erweiterung der Forschung auf dynamische Übungen und die Einführung eines Echtzeit-Knieachsenverfolgungsalgorithmus, der an Störungen anpassbar ist. Praktische Implikationen für die Erkennung von Aktivitäten und die Überwachung des Bewegungsumfangs bei Knierotationen werden hervorgehoben. Die Studie legt den Grundstein für zukünftige Forschung zur Verbesserung der Robustheit und Anwendbarkeit in vielfältigen biomechanischen Szenarien.

Nataliya Didukh, Ihor Zhvanko

Title of Thesis

Human joint angle measurement exploiting kinematic constraints using an inertial motion capture system

Keywords

IMU, joint, angle, hinge, ART, optical capture, inertial capture, kinematic constraints, optimization, particle filter

Abstract

Accurate measurement of human joint angles is critical in biomechanics, impacting fields like sports science and rehabilitation. This thesis introduces a calibration method for joint angle measurement with inertial motion capture system using Particle Filter methods, aiming to enhance real-time angle measurement accuracy.

The methodology employs Sequential Importance Sampling to determine flexion/extension axes of the knee joint using two Inertial Measurement Units (IMUs). The best estimate of the knee joint is then used to measure knee flexion/extension angle. Results demonstrate a remarkable roughly 4° RMSE compared to optical capture, with the algorithm proving stable across varied sensor placements and exercises.

Contributions include extending research to dynamic exercises and introducing a real-time knee axis tracking algorithm adaptable to perturbations. Practical implications for recognizing activity and monitoring Range of Motion in knee rotations are highlighted. The study sets the groundwork for future research in enhancing robustness and applicability in diverse biomechanical scenarios.

Contents

List of Figures

List of Tables

1 Introduction

by Nataliya Didukh, Ihor Zhvanko

In biomechanics, achieving accurate measurements of human joint angles is important for a diverse range of applications. Various studies [62, 39, 28, 29, 30], define a *joint angle* by the single, two or three dimensional Euler angle(s) between two adjacent bones connected by a joint. The dimensionality of the angle corresponds to the *degree of freedom* (DoF) of the joint. The human body exhibits single DoF joints (such as hinge and pivot joints, e.g., elbow, knee, neck), two DoF joints (including condyloid and saddle joints, e.g., thumb, wrist), and three DoF joints (like ball-and-socket joints, e.g., hip joint).

Accurate measurement of these angles is crucial not only for understanding biomechanical movements but also for informing fields such as sports science, rehabilitation, and ergonomics. These measurements provide valuable insights into the mechanics of human motion, facilitating the development of effective interventions, training programs, and ergonomic solutions. For example in [58, 59], the joint angle helps to increase substantially the performance of a functional electrostimulation (FES) of paralyzed muscles to regain functional movements. Moreover, the human joint kinematics is relatively complicated to assess directly, therefore different methods are used to simplify and represent the complex movements of human body called modeling techniques. The modeling technique that represents the joint kinematics through linked-rigid bodies connected by joints with varying DoF is actively employed in numerous studies [24, 37, 66, 64].

Since the Euler angle(s) by definition are successive planar rotation angles around x, y, and z axes of the coordinate system (also referred to as *reference frame*), a body-fixed joint coordinate system (JCS) is required for consistency in reporting the joint angles. Grood and Suntay [24] proposed first JCS for a knee joint in 1983. Following the similar approach, the International Society of Biomechanics (ISB) defined JCS for almost the entire body [63, 62] specifying the reference axes of JCS's characterized by palpable or identifiable anatomical landmarks. The axes identified via anatomical

landmarks are generally referred to as *anatomical axes* [53]. The ISB guidelines prompted researchers [45, 56, 53] to apply prospectively these definitions to report the joint motions in clinically relevant terms.

As these guidelines hardly depend on the positioning of anatomical landmarks, optical capture systems prove to be well-suited for recording kinematic data within a laboratory setting. Yet, assessing and recognizing daily physical activities typically entail challenges outside conventional laboratory settings [23, 52], unless the subject resides within a laboratory environment, a circumstance that usually requires an additional effort. Considering this, inertial motion capture systems are currently being utilized to evaluate human activity beyond the laboratory environment [10, 19]. The (magnetic) inertial measurement unit ([M]IMU) lacks the capability to measure spatial position accurately. Unfortunately, this limitation hinders the precise estimation of anatomical axes and, consequently, the establishment of a JCS as described in the ISB guidelines for capturing joint angle(s). Noteworthy is that, an IMU equipped with a magnetometer, can effectively measure parameters such as linear acceleration, angular velocity and orientation, offering valuable data distinct from spatial position measurements. Furthermore, under specific conditions, a set of (M)IMUs enables the derivation of a joint's rotational axis and the center of rotation(CoR) [16], which may be used as counterparts in inertial capture for anatomical axes in an optical capture system. In a recent study [65], the disputable association between the knee rotational axis (FEA - also referred to as a knee functional axis), and two major anatomical axes (i.e. the transepicondylar axis [TEA] and the cylinder axis [CA]) was investigated. The authors concluded that both anatomical axes deviate from the functional axis in terms of angular displacement, while the CA is the closest axis to the FEA and can serve as an anatomical surrogate for the functional knee axis. Considering that, the data acquired via optical motion capture is not directly translatable to inertial motion capture systems even though the former is normally used as a gold standard.

In the literature, (M)IMUs capture researchers' attention as an available and cheap alternative to complex motion capture systems [8]. Still, inertial motion capture systems have some limitations such as a reduced accuracy due to acceleration and magnetic disturbances, arbitrary sensor orientations relative to actual physical orientations, and sensor alignment with any anatomical frame outlined in ISB guidelines (*anatomical calibration*). Anatomical calibration normally requires a strict protocol and is performed prior to any angle measurements. The aim of this thesis is, therefore, to develop an improved method for conducting anatomical calibration concurrently with real-time angle measurement without imposing any sensor alignment constraints or necessitating a strict

calibration protocol. Ultimately, the accuracy of the presented method was assessed by comparing the estimated joint angle to the optical capture system under various static and dynamic conditions.

This thesis is structured into five chapters. After the introduction, Chapter 2 conducts a comprehensive literature review and introduces the problem statement. Chapter 3 outlines the methodology employed to address the problem, encompassing the mathematical foundation and a probabilistic algorithm. In Chapter 4, participants, experiments, and results are thoroughly detailed. Finally, Chapter 5 delves into a discussion of the results, highlights noteworthy findings, concludes the thesis, and proposes directions for future research.

2 Analysis

2.1 Motion Capture in Human Kinematics Analysis

by Nataliya Didukh

Richard Backer [4] emphasizes that rehabilitation belongs to a clinical discipline in which clinical tests and research are conducted to assess the severity of abnormality, make a treatment decision, determine prognosis, and possibly avoid intervention. In this respect, the quantification of human joint kinematics plays a substantial role in clinical movement analysis for a purpose of rehabilitation, diagnosis of lower-/upper-limb diseases, and monitoring the patient in neuromuscular conditions (e.g., Cerebral palsy, Parkinson's disease).

Besides the movement analysis, the assessment of lower-/upper-limb kinematics went beyond the laboratory and is utilized for performance optimization and injury prevention in sports. In cycling, the change in a knee flexion/extension angle has a clear correlation with anaerobic mean power output and helps to identify the potential drop in performance. Concomitantly, the excessive deviations of the knee flexion/extension angle due to erroneous saddle height soar the traumatic risk [10]. In skiing, mobility assessment of the lower extremities is essential for the same reasons [19], especially outside the laboratory in a harsh environment and at elevated speed.

In human robotics [27] for example, the human kinematics assessment contributes to the exoskeleton's awareness of human kinestate [14] and thus results in smart and accurate assistive and/or rehabilitative action during physical human-robot interaction scenarios.

Although the discussion on reasons behind human kinematics, human joint kinematics has a descriptive nature, and it requires the choice of meaningful biomechanical measures. According to evidence-based clinical practice [1], each biomechanical measure can be validated, which ultimately implies the repeatability and accuracy of the measure.

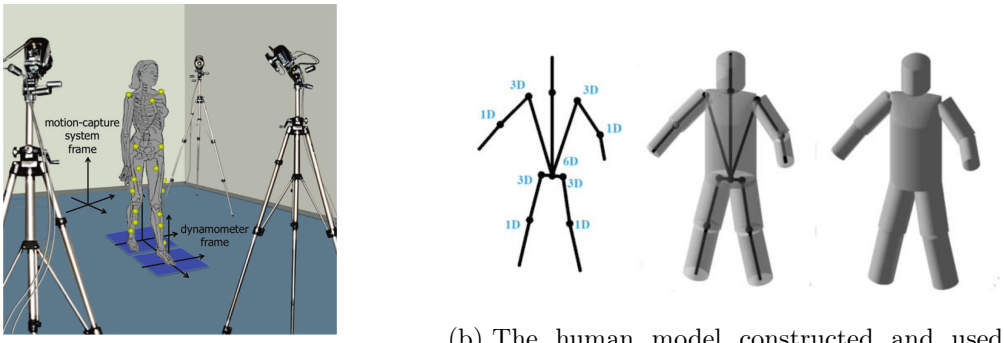

(a) Typical marker-based optical capture system.

(b) The human model constructed and used in [68] to track human motion in real-time.

Figure 2.1: Optical capture system and human model.

Various systems were developed and actively adopted for measuring human body kinematics and dynamics. To assess the human joint angle, particularly non-invasive technologies such as goniometers, inertial, and optical motion capture systems attract researchers' attention.

2.1.1 Marker-based Optical Motion Capture

The typical marker-based optical capture (stereophotogrammetry) relies on a set of markers (e.g., retrospective) generally attached to anatomical landmarks on body segments. These markers' instantaneous positions, orientation, and trajectories are tracked by one [40] or several [6] high-quality infrared cameras (see Figure 2.1a). Optical capture is capable of reconstructing the skeletal system and, when combined with accurate morphological information (e.g., the location of anatomical landmarks), facilitates advanced kinematic analysis [6]. Having the reconstructed skeletal system, the data allows to calculate joint angles. However, assessing kinematics with marker-based optical capture involves controlled laboratory settings, trained staff, and costly facilities, limiting its application for daily life activities.

2.1.2 Marker-less Optical Motion Capture

To avoid the inconvenience of wearing obtrusive on-body markers, marker-less optical capture is designed to track the subject using one or multiple depth cameras (e.g., Kinect sensors) [68]. The detection and tracking process require a human model that imposes

(a) Goniometers for Human Kinematics Assessment.

(b) Exoskeleton for Human Kinematics Assessment.

(c) Human Model for Motion Analysis.

Figure 2.2: Exploring diverse motion capture systems: goniometer, exoskeleton, and IMUs utilizing a human model.

constraints on the 3D appearance of the human (see Figure 2.1b). The human model typically employs a kinematic tree model consisting of joints and body parts with an origin in the pelvis, and an extended cylinder model for the body shape. However, markerless systems include expensive depth sensors (e.g., time-of-flight cameras, structured-light systems) that have a limited measurement volume. Additionally, monocular setups are prone to occlusions, although the multi-view approach may mitigate this problem at an additional computational cost.

Optical motion capture has proven to be the *gold standard* [48] in dynamic motion analysis, achieving high resolution and sub-millimeter accuracy with proper calibration. Nevertheless, a common source of error during application is the inaccurate identification of anatomical landmarks (e.g., medial and lateral epicondyle for the knee), which usually requires palpation performed by a specialist. Despite its remarkable accuracy, optical capture, due to its constrained tracking volume and expensive laboratory setup, is not practical for assessing human kinematics in daily living. Monitoring and tracking human kinematics in everyday life is essential, for example, to reveal crucial information that is missed when measuring motor symptom severity with traditional in-lab methods, as indicated by a recent study on Parkinson's disorder [23].

2.1.3 Goniometer Motion Capture

The introduction of lightweight exoskeletons (see Figure 2.2b) and flexible goniometers (see Figure 2.2a) facilitates the quantification of human kinematics in unconstrained environments. Exoskeletons usually build out of metal or plastic bars and are generally linked with potentiometers, goniometers, or rotational encoders at the joints. Rigidly attached to the body, the exoskeleton moves with the object, which supports the movements, reducing the traumatic risk, and provides feedback on human kinematics [61]. Nevertheless, the mechanical attachments affect the range of motion of the human joints which remains a significant drawback for a wide range of applications. In contrast, the flexible goniometers improve wearability and has reduced interference with natural human movements. However, both wearable systems still suffer from cumbersome setup procedures and misalignment of mechanical rotational axis with anatomical axes.

2.1.4 (Magnetic) Intertial Motion Capture

Magnetic and inertial motion capture has gained significant interest in the field of biomechanics [48], owing to technological advancements in microelectromechanical systems (MEMS) that have led to subsequent miniaturization, optimization of power consumption, and integration with wireless technologies. One or multiple inertial measurement units (IMUs) are attached to body segments, combining a 3-axis gyroscope and accelerometer to measure angular velocity and linear acceleration along three orthogonal axes (the technical coordinate system), respectively. Moreover, many studies incorporate devices so-called (M)IMUs with a 3-axis magnetometer measuring the local magnetic field.

The orientation of the sensor's technical frame with respect to a global reference frame is typically estimated using fusion algorithms such as the Kalman filter or complementary filter [46]. Subsequently, the sensor unit enables tracking and analysis of acceleration, rotational movements, and orientation of body segments. In contrast to marker-based optical motion capture, inertial capture imposes no specific requirements for the placement of (M)IMUs on body segments. However, Niswarder et al. [41] have confirmed variations in bias and root-mean-square error (RMSE) values depending on the sensor attachment.

Due to their low cost, good wearability [35], unrestricted measurement volume (e.g., outdoors), and real-time operation, (M)IMUs are predominantly applied in fall detection systems (FDS) [42], human-machine interface (HMI) [27], human activity recognition

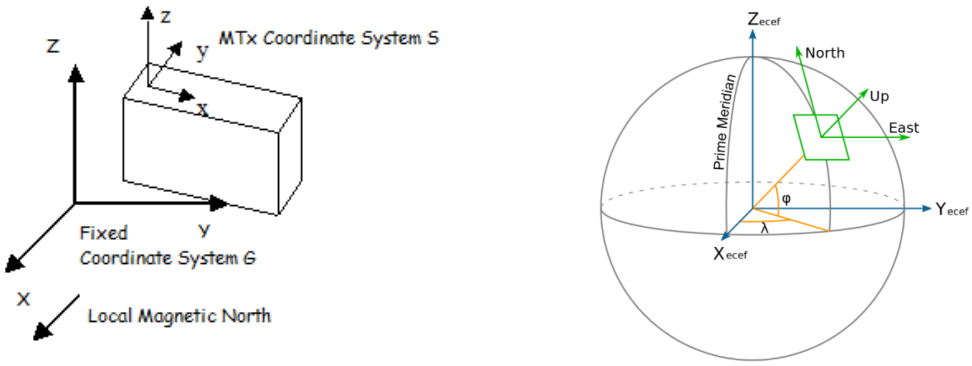

(a) Orientation of a sensor's technical frame relative to a fixed (global) coordinate system. (b) Earth Coordinate System Representation.

Figure 2.3: Technical and Global Reference Frames.

(HAR) [5], human locomotion analysis [47], human posture tracking [3], and sports science [10]. Unlike all the aforementioned approaches, inertial capture requires a more straightforward setup procedure and has minimal interference with natural human movement.

The estimation accuracy is a critical issue that hinders widespread application. In addition, the soft-tissue and muscle movement artifacts are also unavoidable. In this regard, optical motion capture has developed several analytical models [22] to compensate soft-tissue artifacts.

2.2 Orientation Estimation of M/IMU

by Ihor Zhvanko

The human joint angle estimation follows normally the standard procedure that includes several steps that are described in detail in the next sections. After the segment-to-sensor calibration (see Section 2.5) is accomplished, the angle measurement relies on the orientation of (M)IMU technical frames relative to a common reference frame. The orientation error of IMU relative to a common reference frame is one of the common error sources which affects human joint angle measurements [18].

In multiple studies [49, 20, 67], researchers utilize the Earth frame (see Figure 2.3b), also referred to as the *absolute orientation*, to track the orientation of adjacent body segments. The noisy but drift-free absolute orientation can be derived from a three-axis

accelerometer and magnetometer by measuring the gravitational force and magnetic field of the Earth (also referred to as heading, azimuth, or North), respectively.

However, the accelerometer senses linear acceleration of the object in addition to gravity, and the magnetometer is susceptible to magnetic inhomogeneities. Therefore, dynamic conditions and magnetic distortions inhibit reliable orientation tracking. Additionally, typical human motion is unlikely to stay in dynamic conditions for an extended period, while the environment remains magnetically inhomogeneous. Thus, compound acceleration is believed to be a less severe issue than magnetic distortion [32].

To address the issue in dynamic conditions, the gyroscope is leveraged to obtain orientation by integrating angular velocity along three measurement axes. However, the noise and intrinsic bias of the gyroscope can only provide reliable orientation for a limited period (e.g., up to two minutes for skiing [19]) due to low-frequency integration drift. Being highly condition-dependent, orientation is normally estimated by different sensor fusion algorithms that leverage acceleration, gyroscope, and magnetometer measurements [31, 32, 55].

In the context of joint angle measurements, where one or more (M)IMUs are attached to body segments, the kinematics of the human joints can be utilized to eliminate the need for a magnetometer. Furthermore, magnetic inhomogeneities and dynamic conditions have the same impact on two or more sensors when they are in close proximity, which is typically leveraged in joint angle measurement.

To effectively fuse the sensor data from an accelerometer, magnetometer, and gyroscope for orientation tracking relative to the Earth frame, a variety of fusion algorithms were developed among which were complementary filter and Kalman filter [32].

A complementary filter is a simple approach often applied in the flight control industry [44] to fuse at least two sources where one has a high-frequency noise (noisy but without drift) and another a low-frequency noise (noiseless but with drift). The basic structure of the complementary filter is shown in Figure 2.4 where two noisy signals pass through low-pass $G(s)$ and high-pass $(1 - G(s))$ (referred to as *complement*) filters. In practice, the complementary filter is found in the following form:

$$angle(t) = (1 - \alpha) \cdot (angle(t - 1) + gyroscope \cdot dt) + \alpha \cdot accelerometer.$$

The coefficient alpha acts here as a parameter to low- and high-pass filters. Owing to its straightforward structure Complementary Filter (CF)-based techniques have the

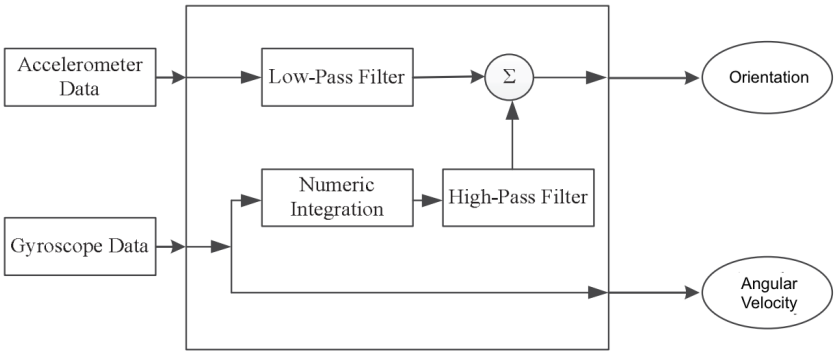

Figure 2.4: Schematic block diagram illustrating the Complementary Filter for sensor fusion in orientation estimation.

advantage of being computationally efficient. However, acting purely in the frequency domain, the filter does not consider any statistical description of noise e.g., Gaussian Noise, White Noise, etc.

2.3 Joint Angle Measurement

by Ihor Zhvanko

Assuming the alignment of a sensor's technical frame to the anatomical frame is determined, the precise and correct way to measure and track joint angles needs to be implemented. Cheng et al. [8] identify four different methods to measure joint angles with (M)IMUs. All four methods rely on rigid-body kinematics to estimate joint angles. Although the authors consider joint angle measurement in the context of robotics as an alternative to magnetic/optical rotary encoders, these methods are actively used in measuring human joint angles on non-rigid human bodies. Since rigid-body kinematics is only an approximation to the human body, angle estimates may deviate due to soft-tissue artifacts. In this section, the methods are described in the context of measuring human joint angles.

2.3.1 Common Mode Rejection

The common-mode-rejection (CMR) method originates from electronics whose idea is to eliminate measured common noise or offset through the signals' difference [8]. The algorithm employs two (M)IMU mounted on adjacent body segments and attached to

arbitrary distance from the joint center. In this case, both sensors measure the same acceleration and magnetic vectors under quasi-static rotational conditions (segments are not rotating around the joint center). Both sensors are in close vicinity, which suggests the same magnetic distortion. In addition, both IMUs sense identically the body's linear acceleration and gravity, which lets assume the same acceleration offset.

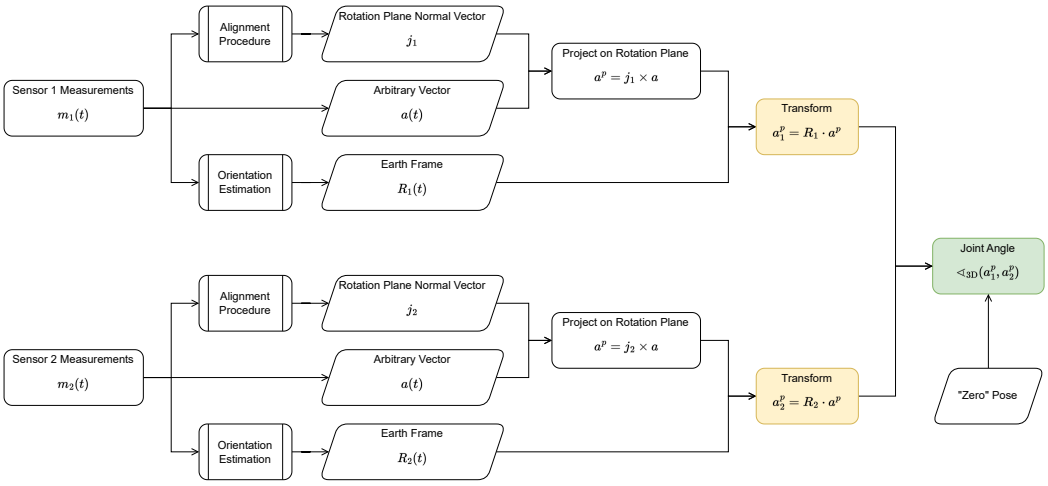

Figure 2.5: Normally, the joint angle measurement setup looks schematically the following way when employing the CMR method. The algorithm usually ingests the (M)IMU measurements to estimate the rotation axis/plane (see Section 2.5) and orientation (see Section 2.2). The arbitrary vector $a(t)$ is usually chosen once at the beginning. Once the projection onto the rotation plane is calculated, the vectors are transformed into a common reference frame. This transformation marked with yellow is the core principle of the CMR method.

The Earth frame estimated from both sensors in this regard must be the same. Assuming that the plane(s) of rotations in sensors' technical frames is determined through the alignment procedure, the joint angle can be derived by selecting an arbitrary vector in each sensor frame (see Figure 2.5). The vectors are projected onto the plane of rotation in the corresponding sensor frame, following which the projections are transformed into a common reference frame (Earth frame). Ultimately, the angle between the projections in a common reference frame differs by a constant from a joint angle. This constant is determined during a *zero pose* - the pose where the joint angle is known.

O'Donovan et al. [45] applies this method through defining common reference vectors relying onto the same assumptions the CMR method does. Favre et al. [20] use a different alignment procedure than O'Donovan et al. but the joint angle is measured

the same way using the CMR method and the zero pose. The application of the method is also found in [49, 56, 50, 64] although the most papers' purpose is alignment procedure improvements.

2.3.2 Common Mode Rejection with Gyroscope Integration

The algorithm as CMR includes two (M)IMU attached to adjacent body segments. O'Donovan et al. [45] emphasize that the total acceleration of the segment measured by a sensor is the sum of body linear acceleration a_L, body rotational movement a_{rG}, gravity g and local rotational movements a_{rL} of the segment.

$$a(t) = a_L + a_{rG} + a_{rL} + g \tag{2.1}$$

Both sensors, according to CMR assumptions, experience the same linear, global rotational, and Earth acceleration. However, due to the local rotational movements of the body segment, the CMR method degrades substantially.

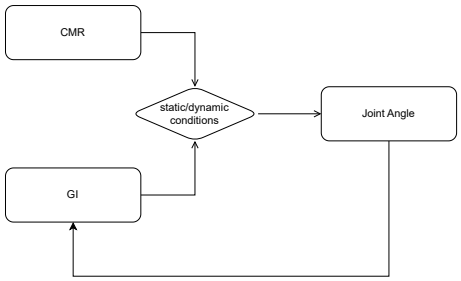

Figure 2.6: CMR with gyroscope integration (GI).

At this point, a distinction is made between local quasi-static and dynamic rotational conditions. Under the first conditions, the acceleration induced by local rotations is negligible or equal to zero, and the CMR method is applied. Once local rotations are detected, the angle measurements are solely based on gyroscope integration, hence the method is named CMR with gyroscope integration (see Figure 2.6).

The GI method utilizes the axis of rotation and angular velocity to estimate the change in joint angle. When used independently, without CMR, it necessitates a zero pose to estimate the angle (see Figure 2.7). The numerical integration in this method also presents the typical challenge of reduced accuracy over time, primarily due to the offset drift and noise in the gyroscope's output.

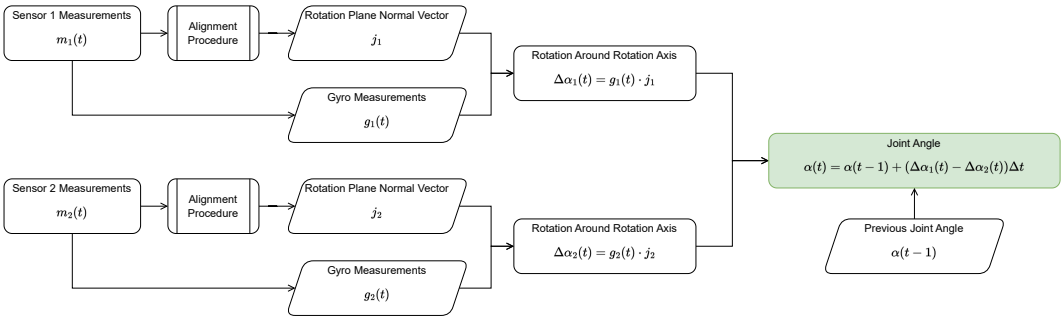

Figure 2.7: The GI method ingests gyroscope measurements, and calculates dot product with a joint axis (see Section 2.5). The angle change is added up to the last known value.

In addition, the significant issue involved in the CMRGI method is that the threshold value must be set to distinguish between static and dynamic situations. In general, this is usually heuristically performed and may prove troublesome. Different papers define this threshold value in different ways:

- Williamson et al. [60] set a threshold on the variance of measured acceleration;
- Ohtaki et al. [43] set thresholds on both the variance and the frequency of the measured acceleration;
- Mayagoitia et al. [37] did not mention this threshold setting at all;
- Dejnabadi et al. [13] set a threshold value on the magnitude difference between the measured acceleration and the gravity;
- O'Donovan et al. [45] set a threshold on the accelerometer and gyroscope as well.

2.3.3 Common Mode Rejection with Gyroscope Differentiation

The method, like the previous ones, utilizes the same hardware setup. Dejnabadi et al. [12] proposed an algorithm based on gyroscope differentiation, hence the name CMRGD. The underlying idea is to estimate local rotational acceleration (see Equation 2.1) by incorporating the vector from a sensor to the joint center, denoted as $\vec{r}$, and gyroscope measurements, avoiding the need for gyroscope integration. The total local rotational acceleration is the vector sum of tangential and centripetal accelerations:

$$a_{rL}(t) = a_T + a_C = \dot{g}(t)M(-\pi/2) \cdot \vec{r} - g^2(t) \cdot \vec{r}.$$

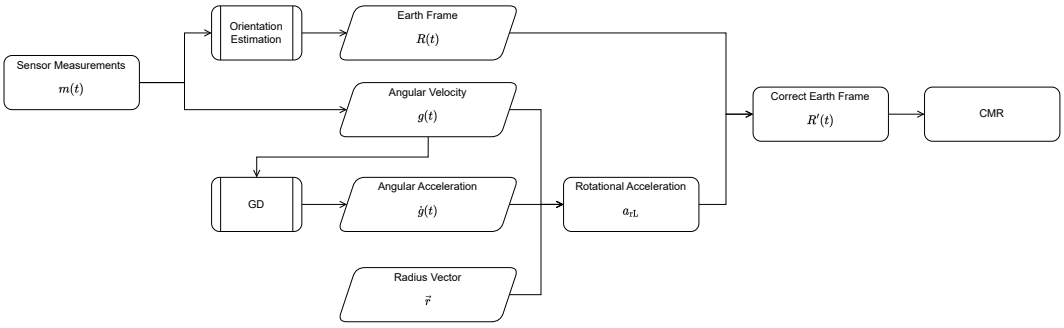

Figure 2.8: The GD method ingests gyroscope measurements along with the vector from a sensor to joint center, and estimates local rotational acceleration. The induced locally acceleration is then deducted from measured acceleration to build a common reference frame.

The local rotational acceleration is deducted from the measured sensor acceleration to apply CMR method (see Figure 2.8). The first challenge in this approach is to measure the vector $\vec{r}$. In [12], the authors use camera, pre-defined static postures and geometry to estimate this vector. Apparently, the approach to measure the vector is not precise and becomes additional error source in joint angle measurement.

Moreover, the numerical differentiation $\dot{g}(t)$ in this method gives the typical problem of a noisy result for angular acceleration. However, it does not have the error accumulation problem as is the case in the CMRGI method with numerical integration, so although much noisier, its calculation error is bounded over time. Utlimately, since the CMRGD method does not have any threshold value to set, it is more straightforward to implement than the CMRGI method.

2.3.4 Distributed Common Mode Rejection

This method, reported in [59], requires two (M)IMUs on each segment to assess the joint angle. The term *distributed* CMR is coined from the approach where acceleration is measured at two positions on the body segment. The method relies solely on the relative position vector between the two sensors.

In this thesis, the setup includes only a single sensor for each segment, hence the DCMR method is mentioned only for completeness without getting into detail. For more details see [8].

2.4 Sensor-to-segment calibration

by Nataliya Didukh

The sensor's *technical frame* is the coordinate system used by the sensor to measure and report data, defining its axes and orientation. The sensor's technical frame is not aligned with neither the meaningful anatomical nor functional axis of a joint or bone segment. Although, the relative orientation between the sensors' and segments' frames serves as a prerequisite for assessing human kinematics in particular joint angle measurement. In the literature, the process of aligning two frames is referred to as sensor-to-segment (S2S) calibration [48]. Researchers normally examine the performance of the S2S calibration methods on the lower-body segments [48][46], although algorithms are fundamentally not constrained to either upper- or lower segments.

Optoelectronic systems utilize precise position and linear trajectory tracking to capture the locations of anatomical landmarks. Once the positions of these palpable body landmarks are obtained, researchers infer the body-fixed JCS following ISB recommendations. Unfortunately, (M)IMUs provide only the sensor's orientation, which precludes the direct application of these recommendations. Nevertheless, under several assumptions, (M)IMU measurements generally allow the determination of functional joint axes in most cases.

The choice of a methodology for S2S involves considering various criteria, including accuracy, repeatability, and usability. Accuracy and repeatability are often assessed by comparing with a reference segment axis, but their importance may vary depending on the application, joint, or movement plane. Studies may prioritize joint range of motion, kinematic patterns, or repeatability based on specific objectives, such as evaluating post-surgery rehabilitation or analyzing joint coordination in sports activities. Usability considerations include the characteristics of the analyzed population, such as physical limitations, which may impact the appropriateness of certain approaches. Additionally, factors like the time available for calibration, influenced by subject fatigue or availability, play a crucial role in method selection.

2.4.1 Static Calibration

Typically, static calibration involves a set of predefined static postures (see Figure 2.9). Each posture, during the calibration procedure, helps identify at least one segment axis.

For example, Favre et al. [20] adopt a standing posture to align thigh and lower leg frames with a gravity vector measured by accelerometers.

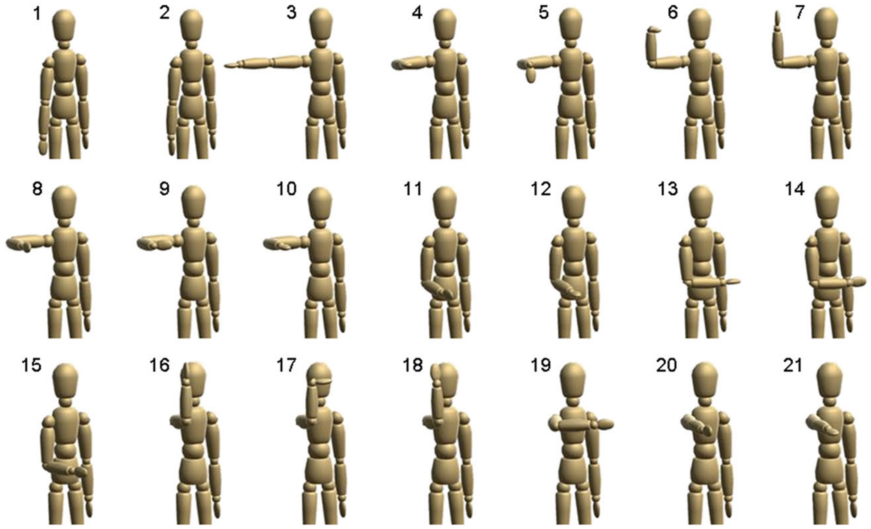

Figure 2.9: Static Postures used in Static Calibration [67].

However, it is important to note that, both in calibration postures and calibration motions, the accuracy is limited by the precision with which the subject can perform the postures or motions.

2.4.2 Functional Calibration

Functional calibration takes advantage of the so-called *pure rotations* [20]. Since a pure rotation, by definition, occurs in one plane, the gyroscope measures the angular velocity perpendicular to this plane. The derived vector from gyroscope measurements is assumed to be parallel to a segment's functional axis.

For example, O'Donovan et al. [45] describes a two-phase functional calibration procedure for lower limb analysis. The authors estimate the anatomical axes of ankle employing two body segment rotations around: the longitudial axis of lower leg and the knee flexion axis. In contrast, Favre et al. [20] ask examiner to perform rotations of a lower leg since the subject may struggle to maintain correct pose and accurately perform a whole-body rotations. Cutty et al. [11][21] went further and developed the *Outwalk protocol* for (M)IMU functional calibration. Although the protocol is the most complete

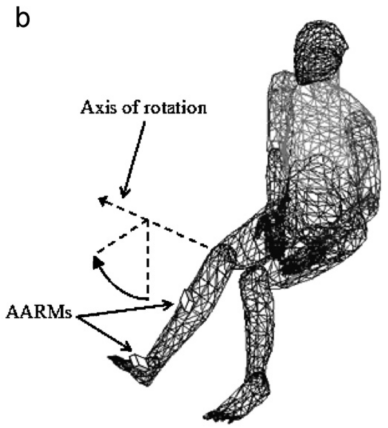

Figure 2.10: Pure rotations used in Functional Calibration [45].

in terms of segments involved, precisely described and easy to perform, the sensors in the procedure require the precise placement. The slight sensors' position deviation cause the a degradation of experimental data.

However, it is important to note that, both in calibration postures and calibration motions, the accuracy is limited by the precision with which the subject can perform the postures or motions.

2.4.3 Anatomical Calibration

Inherently, the most accurate method to achieve S2S calibration for (M)IMUs is described by Picerno [49]. In short, an IMU and an optical marker (referred to as the calibration device) are attached together onto a body segment (see Figure 2.11). The orientation of a sensor's technical frame relative to the calibration device is known. Consequently, the orientation of the JCS relative to the sensor's technical frame can be deduced from the calibration device orientation.

The anatomical calibration relies on external palpable anatomic landmarks. Normally, the expert identifies the anatomical landmarks' location through manual palpation. The procedure is time consuming in comparison to other methods [49].

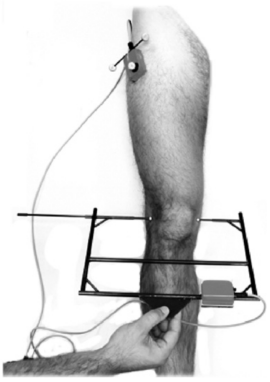

Figure 2.11: Optical markers [49].

2.4.4 Manual Calibration

The manual calibration implies that the (M)IMU's technical frame is perfectly aligned with the anatomical frame. Normally, the trained staff aligns manually the sensors with a meaningful segment axes [12].

2.4.5 Constraint Calibration

In the literature, some authors [50, 28, 64] use an alternative approach to align a sensor's technical frame with functional axes. The main idea is to exploit kinematic constraints to automatically build the alignment, avoiding any pre-defined calibration procedure. In this thesis, this approach is referred to as 'constraint calibration.'

Young [66] applies body model constraints to improve the accuracy of inertial motion capture. The author leverages joint kinematic constraints and gyroscope measurements to correct accelerometer-based orientation. The study demonstrates how considering kinematic restrictions enhances orientation tracking for motion reconstruction. Similar applications of kinematic constraints for orientation correction are found in [29, 30, 31].

Seel et al.[51] introduce a novel method for calibration exploiting kinematic constraints. The authors adopt kinematic constraints for 3-DoF joints (spheroidal joints) and 1-DoF joints (hinge joints) to align (M)IMUs' technical frames and body frames. The hinge joint is assumed to approximate a knee joint, and the spheroidal joint approximates an ankle joint. In another study [50], Seel et al. recall the same alignment procedure and apply it to joint angle measurements using two different approaches, with and without

a magnetometer. Müller et al. [39, 28] follow a similar approach to extend Seel's work and build a kinematic constraint for a 2-DoF joint (elbow joint). Chen et al. [7] describe kinematic constraints for a 2-DoF joint (hip joint) and a 1-DoF joint (knee joint) to estimate angles in lower-limb segments. Additionally, the authors in [39, 7] rely on a zero pose to define a baseline for angle measurement, as mentioned before, the pose by which the joint angle is known.

The calibration procedure based on kinematic constraints for 3-DoF joints is actively researched. As mentioned above, Seel et al. [51] introduced a constraint for 3-DoF. However, the constraint does not include anatomical axes that can be later found using optimization algorithms. Yi et al. [64] proposed a universal kinematic constraint for 3-DoF joints, decoupling the rotation into three successive rotations around three anatomical axes. The problem is broken into three optimization sub-problems that ultimately solve the alignment problem.

2.5 Problem Statement

by Nataliya Didukh, Ihor Zhvanko

The problem at hand involves measuring human joint angles using affordable and readily available inertial measurement units (IMUs).

The background of the issue is highlighted in Section 2.5, where it is explained that integrating sensors into clothing results in arbitrary sensor-to-segment orientation. Consequently, specific assumptions about sensor placement cannot be made. Recent works, as detailed in Section , have attempted to deduce the sensor-to-segment orientation from predefined calibration postures and motions. However, the precision of the calibration is limited by the subject's adherence to the protocol, as discussed in Section . Therefore, there is a need for further research and new methods to establish a sensor-to-segment orientation without relying on a strict calibration protocol.

The relevance of the problem lies in the application of Human Activity Recognition (HAR), which has found uses in user-machine interface, athletic performance analysis, rehabilitation, and patient monitoring for detecting abnormal activities (see Section 2.1). As elaborated in Section 2.1, IMUs play a crucial role in human joint angle measurement for HAR, particularly in clinical gait assessment. The literature review underscores the attractiveness of IMUs for HAR applications due to their cost-effectiveness, unobtrusiveness,

and portability. However, a primary challenge remains in selecting the features to extract, dependent on the application domain. Human joint angles, obtained from pairs of IMUs fixed at adjustment segments, serve as a valuable feature for reconstructing and analyzing human posture in specific domains. Addressing this challenge involves developing a probabilistic method to calibrate IMUs for joint angle measurement.

With that in mind, and emphasizing the objectives while expanding on the analysis, this thesis aims to pioneer an enhanced calibration method for real-time angle measurement. This method is designed to operate seamlessly in real-time without imposing stringent calibration protocols or alignment requirements.

3 Method

This thesis proposes a sensor calibration method to determine a flexion/extension axis for measuring human joint angles. In this method, two sensors are attached to corresponding adjacent body segments connected by a knee joint. Kinematic constraints for a hinge joint, introduced in studies [50, 7], are incorporated to formulate an optimization problem for finding a knee functional axis. Examining various methods used to solve the problem, such as least squares [50] and gradient descent [7], this work explores a probabilistic algorithm known as Sequential Importance Sampling (SIS) [2].

This approach enables the extraction of a major rotation axis of a knee joint from two IMUs based solely on gyroscope data, without relying on strap-down integration. The algorithm proves robust against high-frequency noise and vibrations. Its design is grounded in particle filter facilities to iteratively optimize the function as soon as new gyroscope measurements become available. Unlike methods such as [50], our approach doesn't necessitate pre-recorded measurements with so-called *rich movements* [50].

Ultimately, the human joint angle is measured simultaneously with the estimation of the functional axis by the CMRGI algorithm mentioned in Section 2.3, where the best-known estimate of the axis is utilized.

As highlighted in the literature review (refer to Section 2.5), obtaining sensor-to-segment mapping commonly involves pre-defined poses and/or movements, manual alignment of sensors, or the utilization of information from an optical capture system. However, static poses and manual alignment methods prove unreliable, as the calibration accuracy depends on the precision with which a subject can follow a given procedure.

In contrast, optical capture is recognized as a gold standard [48] in angle measurement, offering more precise determination of the anatomical axis. Functional calibration, involving pre-defined movements, is considered a trade-off between the aforementioned methods when appropriately designed. Typically, functional calibration includes movements requiring a joint to rotate in one plane. Since a rotation occurs in a single plane, a

gyroscope should capture the angular velocity perpendicular to the plane of rotation. The measured vectors are then averaged to define the functional axis of the joint.

Exploiting the inherent single Degree of Freedom (DoF) nature of the hinge joint, which rotates exclusively in one plane, is a key aspect addressed in this thesis and expressed in terms of a kinematic constraint. It is noteworthy that, as a single DoF joint, the knee joint is a simplified anatomical model according to [24]. Moreover, in this thesis, soft-tissue artifacts are anticipated and integrated into the model as uncertainties.

Determining the functional axis of a knee joint formulated as an optimization problem facilitates finding the axis without any sensor-to-segment attachment requirements. In conclusion, the method in this thesis relies on the following assumptions:

- Arbitrary sensor-to-segment orientation;
- Arbitrary distance from joint center to a sensor;
- Any strict protocol is not required to estimate sensor-to-segment orientation of sensors;
- Sensor-to-segment calibration is not required before joint angle measurement;
- Uncertainties due to skin and muscle motion effects (soft-tissue artifacts) are acceptable;
- Sensors are recalibrated automatically after slight sensor displacement.

3.1 Equipment and Setup

by Nataliya Didukh

The setup to validate the proposed algorithm incorporates two devices attached to the upper and lower leg connected by a knee joint of a subject. Each device is equipped with an analog gyroscope, accelerometer, and magnetometer with the capability to adjust the effective measurement range and sample rate.

Alongside each (M)IMU is a 6-DOF optical marker securely attached to the device (see Figure 3.1). The optical markers measuring the absolute orientation are part of the optoelectronic system, consisting of 8 cameras operating at a sampling frequency of 60 Hz.

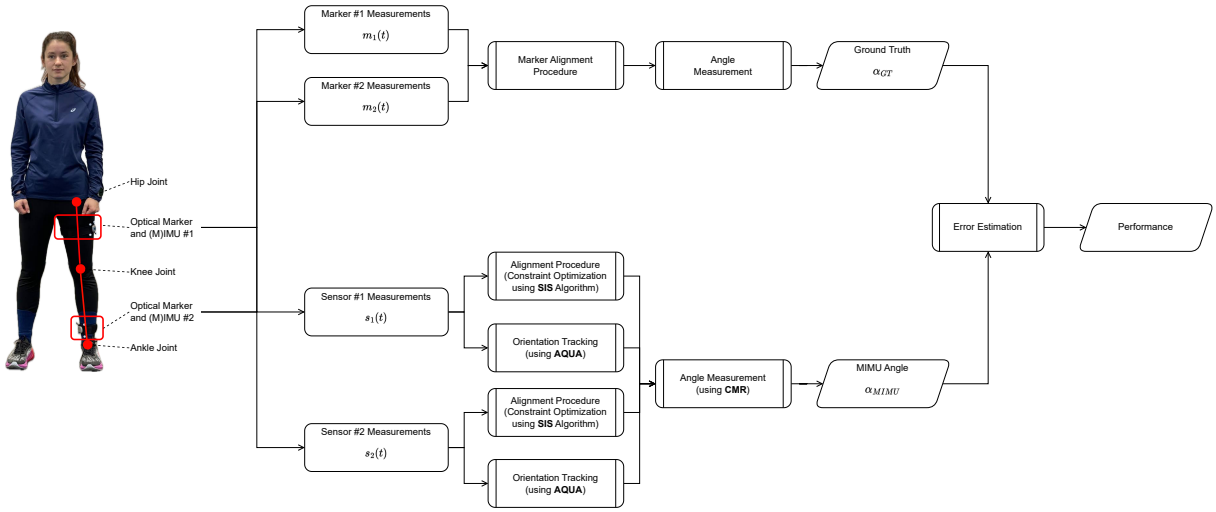

Figure 3.1: The schematic setup of the angle measurement and validation systems. The validation system ingesting the markers data samples estimates the ground truth. Shortly below, the angle measurement system taking the (M)IMUs data samples produces the joint angle that is compared with a ground truth. Utimately, the error allows to assess the joint angle measurement performance.

3.1.1 Participants Information

By forming a cohesive and relevant participant group, specific inclusion and exclusion criteria were employed. Participants were required to be between 18 and 60 years old, possess no history of knee injuries within the last year, and have at least a basic level of fitness to perform the exercises. Individuals with any medical conditions affecting mobility were excluded from participation.

This research did not recruit participants using any particular method or at specific locations. Interested individuals who met the established requirements were invited to participate in the study. Each participant gave informed consent before being involved in the study.

Four individuals who met the criteria willingly participated in the study. The sample size was chosen considering robust data collection, time constraints, efforts, and practical considerations, yet allowing for a comprehensive exploration of the algorithm's performance across the diverse range of participants in the study.

(a) Opening and closing pose of the exercise.

(b) The participant during the gait.

Figure 3.2: Gait experiment.

The age of the participant group ranged between 25 and 45, with a balanced representation of both genders. Detailed demographic information is presented in Table 3.1. All participants were in good health and had the necessary physical condition for the study, with none reporting any current or recent knee injuries.

Participant ID	**Age Range**	**Gender**
001	25-30	Female
002	35-40	Male
003	30-35	Female
004	20-30	Male

Table 3.1: Demographic Profile of Participants.

3.1.2 Exercise Protocol

The participants engaged in a series of controlled exercises designed to comprehensively assess the performance of the angle measurement algorithm. The exercises were carefully selected to simulate real-world scenarios and elicit a natural range of motion, similar to daily activities. Additionally, before the assessment of exercises, participants underwent a brief 30-second warm-up consisting of arbitrary joint mobilization movements without specific restrictions. In the following, an overview of the exercises is presented.

Walking Gait

After the warm-up, participants stood in an upright and relaxed position for 30 seconds before walking to determine sensor orientation when the knee angle is fully extended (straight angle). Subsequently, participants walked along the predefined path at a comfortable pace, completing 3 gait cycles per leg. Finally, the same upright and relaxed position was maintained for the last 15 seconds.

Squatting

Just like during the gait, following the warm-up, participants maintained the upright pose for 30 seconds. Next, the participants performed squats for 6 repetitions to assess the algorithm's accuracy in tracking knee angles under active muscle exposure, and soft-tissue movements.

Figure 3.3: Squats Experiment.

Knee Extensions

After the warm-up and standing upright for 10 seconds, the participants were seated comfortably on a chair with their back straight and feet flat on the floor for 5 seconds. The knee angle was approximately 90 degrees. The exercise began with the participant keeping the upper body stationary, extending fully the right leg to straighten the knee, and then returning to the initial position. The exercise was repeated five times at a relaxed pace, allowing for the evaluation of the algorithm's accuracy during relaxed and controlled movements.

Figure 3.4: Knee Extensions Experiment.

3.1.3 Sensor Placement

Various sensor placement configurations on the upper and lower legs were considered. Participants used a flexible, adjustable wearable band to securely attach the sensor, ensuring relatively consistent sensor placements during dynamic exercises.

The participants wore sensors in three different configurations, as detailed below:

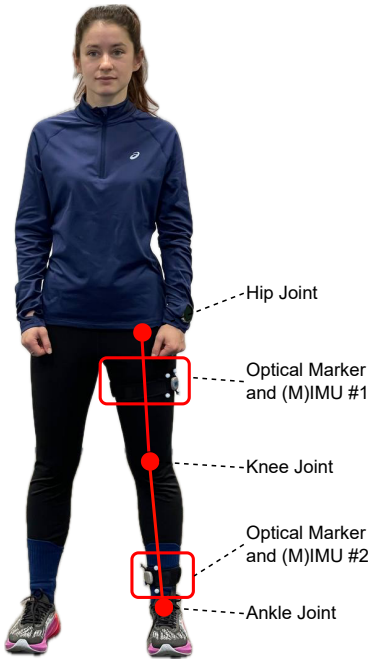

Figure 3.5: Passive markers and IMU sensors placement 003.

Configuration ID	Upper Leg Mounting Point	Lower Leg Mounting Point
001	Away from the knee	Close to the knee
002	Close to the knee	Away from the knee
003	Away from the knee	Away from the knee

Table 3.2: Sensor Placement Configurations.

The different configurations assess the algorithm's adaptability to variations in sensor placement and provide additional insights on algorithm performance considering different proximity from the knee joint.

3.1.4 Sensor Configuration

In every experiment, two MetaMotionS devices from MBIENTLAB [26] were attached to the upper and lower part of the same leg (see Figure 3.5). Each device was equipped with an analog gyroscope, accelerometer, and magnetometer with adjustable sample rate and effective range.

Each MetaMotionS was configured with the following parameters:

Sensor Component	Sample Rate	Effective Range
Accelerometer	100 Hz	±8 g
Gyroscope	100 Hz	±1000 deg/s
Magnetometer	25 Hz	±1300 µT (z-axis), ±2500 µT (x,y-axis)

Table 3.3: Sensor Configuration Details.

The required calibration procedure was conducted in the experimental environment for each sensor to optimize their performance and ensure accurate data collection.

3.1.5 Optical Capture Configuration

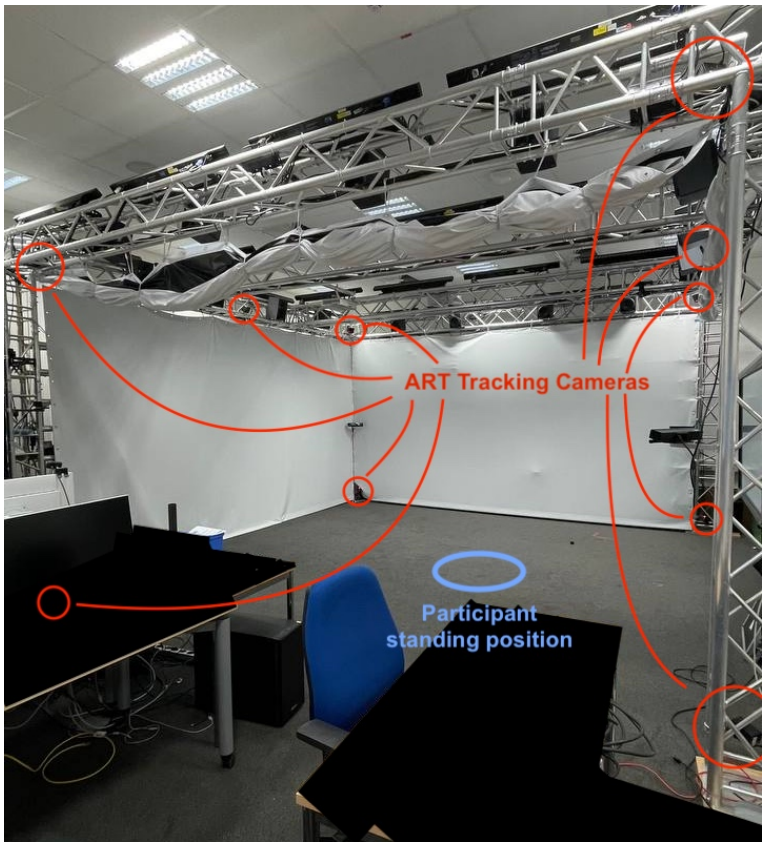

Figure 3.6: ART room with cameras.

In this thesis, the Advance Realtime Tracking (ART) system is utilized as ground truth. The ART system is an optical capture system known for high precision and versatility in

optical tracking. It operates on the principle of recording the positions and orientation of passive markers within a constrained tracking volume.

The ART system comprises 8 high-quality IR cameras strategically positioned around the experimental space to capture the real-time position and orientation of markers. Given the typical challenges of occlusion with on-body markers, a thoughtful arrangement of tracking cameras was implemented (see Figure 3.6). This arrangement maintains a continuous line of sight for all cameras, minimizing instances of occlusion and ensuring uninterrupted tracking of a passive marker throughout the experiment.

In each experiment, two passive spherical retro-reflective markers were positioned on both the upper and lower legs at the exact locations where the IMU sensors were attached (see Figure 3.5). These markers were enveloped with retro-reflecting foils, applying the glass spheres principle to optimize reflectivity. The *hand target* (a passive marker from ART) is a 6-DoF optical passive marker that provides rich data on both position and orientation.

The optical capture system operates at a frame rate of 60 Hz. This frame rate ensures high temporal resolution, capturing rapid movements with the desired precision. The configuration aligned with the experiment's requirements allowing real-time tracking while being computational efficiency.

3.2 Ground Truth

by Nataliya Didukh

The described algorithm captures the dynamics of knee joint rotation by tracking changes in relative orientation and deriving a stable estimate of the knee axis. The choice of a Butterworth filter and a magnitude threshold contributes to the robustness of the algorithm, ensuring accurate knee axis estimation.

3.2.1 Knee Axis Estimation Algorithm

The estimation of the knee axis is a critical aspect of biomechanical studies, providing insights into joint kinematics during various activities. In this section, we present a detailed methodology for obtaining a knee axis using two passive markers, S_a and S_b,

attached to the upper and lower leg, respectively. The algorithm leverages relative orientations and their dynamics to robustly estimate the knee axis.

Sensor Orientations

The orientation of S_a and S_b, represented by R_{S_a} and R_{S_b} matrices, captures the spatial alignment of the sensors attached to the upper and lower leg. These matrices serve as the foundation for calculating the relative orientation between the two sensors.

Relative Orientations

The relative orientation of S_a with respect to S_b ($R_{S_a \to S_b}$) and vice versa ($R_{S_b \to S_a}$) is pivotal for understanding the knee joint's rotational dynamics. The equation

$$R_{S_a \to S_b} = R_{S_b} \cdot R_{S_b}^{-1} \tag{3.1}$$

ensures an orientation agnostic to absolute leg positioning, focusing solely on the relative alignment of the sensors.

Dynamics of Relative Orientation

The knee joint's 1-DoF manifests in the relative orientation undergoing rotations around a consistent axis during knee flexion and extension. This characteristic forms the basis for tracking knee joint dynamics and estimating the knee axis.

Algorithm Steps

The algorithm unfolds in a series of steps designed to capture the nuanced dynamics of the knee joint:

- **Obtain Sensor Orientations**: Acquire the orientation matrices R_{S_a} and R_{S_b} for the upper and lower leg sensors.
- **Calculate Relative Orientations**: Determine $R_{S_a \to S_b}$ and $R_{S_a \to S_b}$ using the equations mentioned above 3.1.

- **Calculate Relative Orientation Changes**: Compute the changes in relative orientations using the difference between consecutive relative orientation matrices (same formular as in the previous step).
- **Convert Changes to Rotation Vectors and Angles**: Apply Rodrigues' formula to convert the changes in relative orientations to rotation vectors and angles.
- **Smooth Rotation Vectors**: Use a third-order Butterworth filter to smooth the rotation vectors obtained for both relative orientations.
- **Filter by Magnitude**: Remove negligible rotations by applying a magnitude threshold (0.01) to the smoothed rotation vectors.
- **Average and Normalize Rotation Vectors**: Average the rotation vectors for both relative orientations and normalize the resulting vector. This normalized vector represents the best estimate of the knee axis.

3.3 Kinematic Constraint

by Ihor Zhvanko

In this thesis, the human knee and elbow each is assumed to have only one rotational degree of freedom. However, both joints are not exactly hinge joints, as they allow some rotation in the frontal and transversal planes, up to roughly 8° [9]. The human leg and arm are modeled as two rigid segments connected by a hinge joint (see Figure 3.7). Two IMU sensors are attached to the segments at an arbitrary distance from the joint center. The orientations of the sensors towards the segments and the joint-related coordinate systems are unknown. Due to the muscles, the sensors cannot be mounted exactly at the segment center; instead, they are positioned at an arbitrary distance from the segment.

According to the model, the algorithm has to handle an arbitrary sensor-to-segment mounting which is the major challenge outlined in Section 2.5.

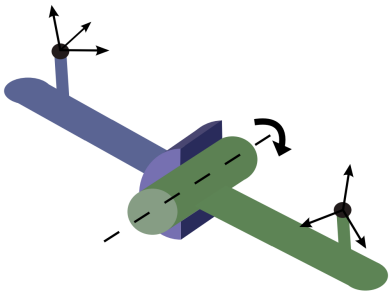

Figure 3.7: The hinge joint model approximates a knee joint [50]. (M)IMUs are elevated at some height from the segment due to soft-tissues.

3.3.1 Symbols and Definitions

Two rigid links with 1-DoF joints are moving in a joint plane $\mathcal{P}_j$. The axis of rotation, denoted as $\vec{j}$, is defined as an identity vector passing through the center of the joint. Additionally, vector $\vec{j}$ serves as a normal vector to the joint plane $\mathcal{P}_j$. By leveraging the properties of the vector cross product, any vector $\vec{c}$ can be projected onto the joint plane, denoted as $proj_{\mathcal{P}_j}(\vec{c}) = \vec{c} \times \vec{j}$. If vector $\vec{c}$ is co-linear with $\vec{j}$, then $proj_{\mathcal{P}_j}(\vec{c}) = \vec{0}$ by definition.

In the following sections, vectors are represented in Cartesian and spherical coordinate systems. Different conventions exist for representing the three coordinates in a spherical coordinate system and for the order in which they should be written. In this work, (r, θ, φ) is used to denote radial distance, inclination (or elevation), and azimuth, respectively, as specified by ISO standard 80000-2:2019. Moreover, we omit r to denote the identity vector $(1, \theta, \varphi) = (\theta, \varphi)$. The inclination θ is constrained to the interval $[-\pi/2, \pi/2]$, and azimuth φ to $(-\pi, \pi]$. Cartesian coordinates can be retrieved from spherical coordinates:

$$
\begin{aligned}
x &= r \cos\varphi \sin\theta \\
y &= r \sin\varphi \sin\theta \\
z &= r \cos\theta
\end{aligned}
$$

The sensors are attached to the segments with arbitrary orientation relative to the segments, and the orientation to common reference frame is known and described via rotation matrices $R_1(t), R_2(t)$ in a right-handed coordinate system.

3.3.2 Hinge Joint Constraint

The hinge joint has an axis of rotation $\vec{j}$ with different coordinates j_1 and j_2 in both sensor coordinate frames. Subsequently, the coordinates of j_1 and j_2 depend solely on the sensors' orientation with respect to the joint. As mentioned earlier, the method doesn't specifically assume that any of the local sensor axes align with the axis of the hinge joint or the longitudinal axis of the segment. Therefore, the direction and position of the knee flexion/extension axis are unknown. According to [51], the axis of rotation can be identified from the measurements of *rich motions* by exploiting kinematic constraints.

The authors adopt the following kinematic constraint for a hinge joint, which is given by:

$$\|g_1(t) \times j_1\|_2 - \|g_2(t) \times j_2\|_2 = 0, \forall t \tag{3.2}$$

where $\|\cdot\|_2$ denotes the Euclidean norm. However, this thesis suggests a system of constraints to improve the tracking accuracy and stability during dynamic motions:

$$\begin{cases} \|(g_1(t) - R_{S_b \to S_a} g_2(t)) \times j_1\|_2 = 0, \forall t \\ \|(g_2(t) - R_{S_a \to S_b} g_1(t)) \times j_2\|_2 = 0, \forall t \end{cases} \tag{3.3}$$

To comprehend the main idea of the constraint, let's break down different basic movements as seen by the sensors. First, picture one sensor staying still while the second one starts moving around the hinge joint. At that point, the first sensor shows 0° angular velocity across all directions, while the second sensor measures an angular velocity of more than 0°. The direction of this spinning speed lines up with the hinge joint axis $\vec{j_2}$. The part of the constraint including $g_1(t)$ becomes 0 by definition, and the second part with $g_2(t)$ also turns out to be 0 (because multiplying co-linear vectors $\vec{j_2}$ and $g_2(t)$ results in 0).

Next, imagine both segments rotate around the hinge joint at the same time with arbitrary angular velocity. The direction of a difference of angular velocities aligns with the hinge joint axis $j_{1,2}$, confirming the constraint.

Now, think about the whole model turning around a spot in space. At this point, both sensors experience angular velocity with the same size. So, the difference of angular velocities must equal to 0° and crossing this with the hinge joint axis, you will get 0°. The constraint stays intact.

Even when you combine these last two movements with linear acceleration, the constraint still holds up.

3.4 Knee functional axis

by Ihor Zhvanko

In [50], the authors collect IMU measurements $S(t), i \in [1, N]$ to estimate the unit-length direction vectors j_1, j_2. However, this approach comes with a drawback the dataset needs to be acquired before angle measurement. Subsequently, a least-square optimization is applied to this dataset. While the computational quality improves with the dataset's growth, there is a significant drop in performance. Moreover, time intervals during which the subject is inactive provide little information for determining the functional axis. In contrast to least squares optimization, where a batch of measurements is processed by finding a parameterized function that best fits the data, Bayesian filters refine the state estimate each time a new measurement is received. Both methods are thoroughly introduced and compared in [38].

In this thesis, an iterative method based on Particle Filter (Sequential Importance Sampling/Bootstrap Filter) is developed to optimize the constraint and overcome the limitations of the least-square approach. Following particle filter algorithms [2], the state vector X is defined as $(\varphi_1, \theta_1, \varphi_2, \theta_2)$ where φ_i, θ_i represent the inclination and azimuth of the functional axis in different coordinate frames j_1, j_2. The objective is to estimate a hidden sequence of the state vector x_k for a static system. Here, *hidden* implies that a direct measurement of the state is unavailable and impossible. Therefore, two additional sources of information are required. The first is a process model describing how the state changes over time, providing prior knowledge about state evolution. The second is a measurement model establishing the relationship between measurements and the process state x_k.

Typically, a particle filter is applied to dynamic models where the evolution of the state over time depends not only on the previous state but also on the input control signal. In the context of this work, *static* implies that the next state does not depend on an input control signal. It is defined as

$$x_k = f_k(x_{k-1}, v_{k-1}) = x_{k-1} + \mathcal{N}(0, \sigma^2) \ , \tag{3.4}$$

where x_{k-1} is the state at the previous time step, and $\mathcal{N}(0, \sigma^2)$ represents process model noise. In this context, the noise is assumed to be independent and constant. Model noise accounts for uncertainty in sensor measurements, soft tissue artifacts, muscle contraction during movement, and model simplifications.

In this thesis, the hinge joint constraint is utilized to define the measurement model for a particle filter. With two sensors attached to adjacent body segments, the measurement model relies on two three-axial sensors that produce six measurements in total: $(\vec{g_1}, \vec{g_2}) = (g_1^x, g_1^y, g_1^z, g_2^x, g_2^y, g_2^z)$. The final measurement model is defined using a non-linear constraint (see Equation 3.3):

$$z_k = \begin{pmatrix} \|(g_1(t) - R_{S_b \to S_a} g_2(t)) \times j_1\|_2 \\ \|(g_2(t) - R_{S_a \to S_b} g_1(t)) \times j_2\|_2 \end{pmatrix}, \tag{3.5}$$

where $j_n = (\cos\varphi_n \sin\theta_n, \sin\varphi_n \sin\theta_n, \cos\theta_n)$ for $n = 1, 2$. Another consideration is that if $g_1(t)$ and $g_2(t)$ are zero vectors, there is no need to perform an iteration, as they do not provide informative data.

3.4.1 Nonlinear Bayesian Tracking

In essence, the problem of tracking is defined as evolution of the state sequence $\{x_k, k \in \mathbf{N}\}$ where the current state is expressed via nonlinear function of the previous state x_{k-1} and noise n_{k-1}:

$$x_k = f_k(x_{k-1}, n_{k-1}).$$

Having the measurements z_k as a function of the current state x_k and measurement noise n_k:

$$z_k = h_k(x_k, n_k),$$

the algorithm must estimate recursively x_k using these measurements (also referred as to observations).

Alternatively, the state estimation problem can be described in probabilistic notation as a Bayesian estimation problem. In a probabilistic sense, the objective of tracking is to recursively calculate some degree of belief in the state x_k taking different values given the measurements $z_{1:k}$. Following the Bayesian approach, the *probability density function* (PDF) $p(x_k|z_{1:k})$ has to be constructed. Besides that, the initial PDF $p(x_0|z_0) = p(x_0)$ of state vector (also referred to as prior) is known. That implies the PDF $p(x_k|z_{1:k})$ may be obtained recursively in two stages: prediction and update.

At the prediction stage, the PDF $p(x_{k-1}|z_{1:k-1})$ is assumed to be available, and incorporates the system model to obtain the prior PDF of the state at time k via the Chapman-Kolmogorv equation:

$$p(x_k|z_{1:k-1}) = \int p(x_k|x_{k-1})p(x_{k-1}|z_{1:k-1})dx_{k-1}.$$

Being modelled as a Markov chain of order one, the current state depends only on the previous step, and mathematically this implies:

$$p(x_k|x_{1:k-1}, z_{1:k-1}) = p(x_k|x_{k-1}),\ p(z_k|x_{1:k}) = p(z_k|x_k). \tag{3.6}$$

In simpler terms, when predicting the state's transition from time $k-1$ to time k, the state x_{k-1} is assumed to contain already all the necessary information. As a result, past states $x_1, \ldots, x_{k-2}$, and previous measurements $z_1, \ldots, z_{k-1}$ are discarded after being processed. A similar principle applies to measurements, as indicated in Equation 3.6.

At the update state, when a measurement z_k at time step k is available, the Bayes' rule is utilized to update the posterior (or prior for the next iteration)

$$p(x_k|z_{1:k}) = \frac{p(z_k|x_k)p(x_k|z_{k-1})}{p(z_k|z_{1:k-1})}$$

where the normalizing constant

$$p(z_k|z_{1:k-1}) = \int p(z_k|x_k)p(x_k|z_{1:k-1})dx_k$$

depends on the likelihood function $p(z_k|x_k)$ defined by the measurement model and the known statistics of n_k. In the update stage, the measurement z_k is used to modify the prior density to obtain the required posterior density of the current state.

The state estimate is expressed as a PDF, capturing both the estimated state and the corresponding uncertainty. The relevant state is termed the posterior state, representing the estimated state at time k considering all measurements and inputs up to time k and past states up to time $k-1$. This is denoted by the conditional PDF:

$$p(x_k|x_{1:k-1}, u_{1:k}, z_{1:k}) = p(x_k|x_{1:k-1}, z_{1:k})\ .$$

3.4.2 Sequential Importance Sampling (SIS) Algorithm

The optimal Bayesian solution leads usually to intractable integrals that can only be solved analytically under strong assumptions. For example, Kalman Filter assumes the posterior density at every time step is Gaussian, and the state evolution and measurement model are linear functions having the Gaussian noise. For the problems where such strict assumptions are inexpedient, the sequential Monte Carlo filters approximate the posterior density through a discrete PDF with no restricts exposed on the models. During the last decades, most sequential MC filters originate from the sequential importance sampling (SIS) algorithm that is in essence a Monte Carlo (MC) method. This sequential MC (SMC) method is also referred to as bootstrapping filtering, the condensation algorithm, particle filtering, interacting particle approximations, and survival of the fittest.

The method involves iteratively using Monte Carlo simulations to construct a Bayesian filter. By generating estimates with random samples and associated weights, the process defines the necessary posterior density function. As the number of samples increases, the Monte Carlo representation converges towards the typical functional definition of the posterior PDF, aligning the Sequential Importance Sampling (SIS) filter with the ideal Bayesian estimate.

First, we have to define a random measure $\left\{x_{0:k}^i, w_k^i\right\}_{i=1}^{N_s}$ that charactirizes the posterior PDF $p(x_{0:k}|z_{1:k})$, where $\left\{x_{0:k}^i, i = 0, \ldots, N_s\right\}$ is a set of support points with associated weights $\left\{w_k^i, i = 1, \ldots, N_s\right\}$ and $x_{0:k} = \{x_j, j = 0, \ldots, k\}$ is the set of all states up to time k. The weights are normalized such that $\sum_i w_k^i = 1$. Following that, the posterior density at k can be approximated as

$$p(x_{0:k}|z_{1:k}) \approx \sum_{i=1}^{N_s} w_k^i \delta\left(x_{0:k} - x_{0:k}^i\right).$$

The pair $\left\{w_k^i, x_{0:k}^i\right\}_{i=1}^{N_s}$ is a set of N_s samples with the corresponding weight where each sample $x_{0:k}^i$ is a possible realization of the state sequence, and weight w_k^i reflects the relative importance of each sample. In other words, the sample having a considerably higher weight relative majority is apparent closer to the true state sequence in contrast to samples with lower weights. Following the law of total probability, the equation implies that the sum of all weights is equal to 1. The function $\delta(x)$ is the Dirac delta function that equals to 0 everywhere except for x, and integral is 1.

The samples, also known as particles (hence the term *particle filter*), represent the posterior as a set of weighted particles. The advantages of the particle filter include the PDF not being restricted to any specific shape, and there are no restrictions on the state evolution and measurement model. However, an insufficient number of particles can lead to poor approximations. Conversely, an increased number of samples results in escalating computational costs. Additionally, the samples must be drawn from a different distribution than the unknown posterior PDF, making direct sampling infeasible. In the SIS algorithm, this distribution is referred to as the importance density q. The importance density is a positive function where the posterior is positive and approximates the weights through the posterior PDF.

Given the importance density q the weights can be expressed via the following expression

$$w_i^k \propto \frac{p(x_{0:k}^i|z_{1:k})}{q(x_{0:k}^i|z_{1:k})}. \tag{3.7}$$

The $\propto$ means that a weight is proportional to the term on the right-hand side that is a ratio between posterior and importance density for an individual particle with index i. This thesis only considers the state at time step k and PDF $p(x_k|z_{1:k})$ rather than the full state sequence $p(x_{0:k}|z_{1:k})$ up to time k. Following that the Equation 3.7 transforms into:

$$w_k^i \propto w_{k-1}^i \frac{p(z_k|x_k^i)p(x_k^i|x_{k-1}^i)}{q(x_k^i|x_{k-1}^i, z_k)},$$

where w_{k-1}^i is the weight at the previous time step for particle i. That implies the approximated posterior can be expressed the following way:

$$p(x_k|z_{1:k}) \approx \sum_{i=1}^{N_s} w_k^i \delta(x_k - x_k^i).$$

When the number of particles is increasing to infinity, this approximation can be shown to converge to the exact solution [6,12,14].

3.4.3 Particle Filter Challenges and Solutions

In this section, the solutions to the five essential challenges of the particle filter are presented. The explained challenges must be addressed before designing and implementing a particle filter for a particular problem.

Degeneracy

The degeneracy problem, also known as depletion, typically arises after a few iterations in particle filters, where one particle acquires a relative weight close to 1, while all other particles have negligible weights close to 0.

This issue, acknowledged as the degeneracy problem, cannot be completely avoided [15]. The variance of the importance weights tends to increase over time, making it impossible to circumvent the degeneracy phenomenon.

The consequences of this problem include:

- A significant portion of the computation cost in each iteration is allocated to calculations involving particles that make negligible contributions to the posterior approximation;
- The posterior approximation effectively relies on a single particle with the highest relative weight, limiting the performance and expressiveness of the filter.

The degeneracy problem results in the divergence of the particle filter due to the amplification of state estimation errors over time.

Before solving the degeneracy problem, the presence and degree of degeneracy should be properly evaluated. For this reason, a suitable measure of degeneracy of the algorithm is the effective sample size N_{eff} and expressed as:

$$N_{eff} = \frac{N_s}{1 + Var(w_k^{*i})},$$

where $w_k^{*i} = p(x_k^i|z_{1:k})/q(x_k^i|x_{k-1}^i, z_k)$ is referred to as the *true weight*. Unfortunately, the exact value can not be obtained, therefore is estimated by

$$\hat{N}_{eff} = \frac{1}{\sum_{i=1}^{N_s}(w_k^i)^2} \tag{3.8}$$

where w_k^i is the normalized weight. The value of $\hat{N}_{eff}$ close to one indicates severe degeneracy.

Once the degeneracy problem is identified, the re-sampling algorithm (also known as dithering) is applied to all particles. Typically, particles with negligible normalized

weights are discarded, while substantial ones are subdivided into smaller particles, often achieved by duplicating the particle. The new particles typically receive weights equal to $1/N_s$.

Figure 3.8 provides a schematic illustration of how a set of weighted particles (where size reflects weight) can be re-sampled into another set of uniformly distributed particles. The re-sampling step can be deterministic or stochastic, determining whether the process is repeatable.

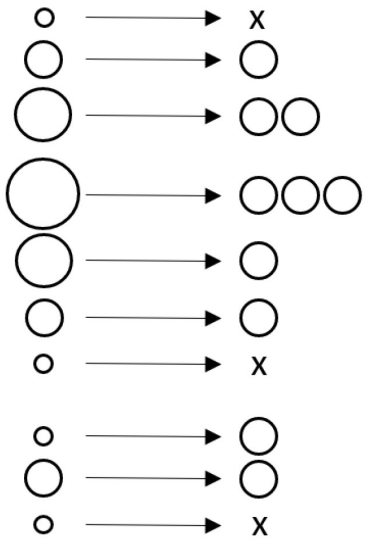

Figure 3.8: Example of how resampling transforms a set of 10 weighted particles (left) into a new set of 10 uniformly weighted particles (right). Some particles are duplicated, while others are never selected and disappear (represented by the x).

All resampling methods can be classified into two categories: sequential and parallel. The parallel implementation executes two or more sequential approaches simultaneously. The sequential implementations are further classified into traditional (or single-distribution sampling), compound sampling, and special strategies [33]. The first two categories are differentiated based on whether the resampling is from a single distribution or multiple distributions via a grouping of the particles.

In this thesis, the residual systematic resampling (RSR) algorithm is employed to resample the particle once the degeneracy is detected. This algorithm belongs to the family of the single-distribution sampling methods where the particle is resampled proportional to

$w_t^{(m)}$ times. The same constraint also referred to as *unbiasedness* or *proper-weighting condition* [36] is described this way

$$E\left(N_t^{(m)}|w_t^{(m)}\right) = Nw_t^{(m)}.$$

The number of particles after a resampling step remains the same and each particle has $1/N$ weight.

However, resampling could have undesirable consequences one of which is sample impoverishment. Low-weighted particles are with high probability dropped during resampling, which lowers the variety of the particles. This problem and selected solution is described in the next section.

Sample Impoverishment

In re-sampling, low-weighted particles are eliminated, and high-weighted ones are repeatedly chosen, resulting in a loss of diversity among the particles. As mentioned before, particle filter methods are based on three operations where, in the first step, the prediction step (or particle propagation) contains both a deterministic and stochastic part (samples are drawn from a PDF). Hence, particles with the same state must diversify during the prediction state. As the process noise decreases, the problem, also known as *sample impoverishment*, deteriorates, and the duplicated samples start to behave as a single particle (see Figure 3.9).

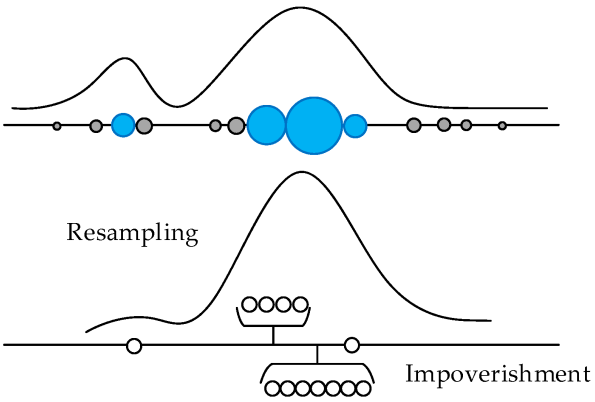

Figure 3.9: A single sample is replicated multiple times, and the cohort of particles behaves as if they are a single point in the state space.

In the worst case, all N_s particles will represent the same state, and again, the filter effectively only has one particle. Like the degeneracy problem, sample impoverishment worsens the filter's performance and causes divergence.

Typically, to address the risk of sample impoverishment, the model is designed to have a sufficient amount of process noise. However, various methods have been developed to mitigate the effect of sample impoverishment even with reduced noise.

The auxiliary particle filter exploits the latest measurements from the update step and preselects samples with anticipated high weights for propagation. This way, the auxiliary particle filter favors well-matched samples for the next iteration instead of randomly generating samples from the prior PDF. Although the algorithm prevents impoverishment, the performance in a higher-dimensional space diminishes, leading to a loss of efficiency in real-time inference.

The most intuitive and easy-to-implement method, known as roughening, to prevent impoverishment was introduced by [34], inspired by Gordon in the Bootstrap Filter (also referred to as dithering in [25]). The authors distinguish between two basic methods:

- *separate-roughening*, which applies artificial noise to the resampled particles;
- *direct-roughening*, which intensifies the process noise of the state propagation step.

While the separate-roughening method implies additional computational effort compared to direct-roughening, it can produce a smoother particle distribution. For this reason, this thesis utilizes the separate-roughening method to mitigate sample impoverishment.

Moreover, it investigates various options regarding the application of roughening and its incorporation into different elements of the algorithm: (i) whether to apply it at all or only at specific time steps, (ii) whether to apply it to all particles or only a subset, and (iii) whether to apply it to the entire vector or specific components. Determining when to apply roughening, the amount of noise to be added, and which dimensions to affect is challenging and lacks a general prescription.

Divergence

The particle filter approach, while an efficient Monte-Carlo method for solving Bayesian tracking problems in non-linear models, can potentially diverge from the true state under certain circumstances in real-world applications. Even though the method may converge

with an increased particle count to ensure result accuracy, this can make the algorithm impractical in real-time scenarios. Consequently, divergence monitoring becomes an essential component in the design of particle filters.

The inherent uncertainty in a model, combined with the recursive nature of the filter, contributes to its instability and susceptibility to divergence from the true state. The three major reasons for particle filter divergence typically include:

- Inaccuracies in the process model that degrade the likelihood of propagated particles with each iteration.
- Higher-than-assumed noise levels in the measurement model, leading to low likelihood for particles that are subsequently removed during the resampling step.
- Incorrect measurements, caused by factors such as sensor faults or outliers, resulting in imprecise estimates.

A straightforward and intuitive approach to monitor divergence is the use of unnormalized likelihoods, focusing on the number of particles with the highest weight. Low likelihoods for each particle in the population, below a specified threshold, serve as a key indicator that predictions deviate from the true state. This simple metric is often sufficient to detect particle filter divergence.

Another metric to estimate divergence is the Kullback-Leibler divergence, also known as relative entropy, which measures the statistical distance between two probability distributions. This metric helps gauge the resemblance or difference between the measurement and estimate. If the resemblance falls below a defined threshold, it suggests that the particle filter has likely diverged [54].

Once particle filter divergence is detected, the current particles are withdrawn, and the filter is reinitialized. This straightforward procedure is effective in recovering the filter from divergence. The algorithm designed in this thesis incorporates divergence monitoring to address unexpected sensor shifts [17].

3.5 Common Reference Frame

by Ihor Zhvanko

The joint angle measurement relies entirely on the orientation of IMU technical frames. However, the orientation of sensors must be referenced to a common frame. Typically, IMUs leverage their ability to sense gravity and magnetic north, making the Earth frame the natural choice for a common reference frame (see Section 2.2). Therefore, estimating orientation relative to the Earth frame becomes a crucial task in joint angle measurement.

The quaternion-based method presented in this section is based on Roberto Valenti's Algebraic Quaternion Algorithm (AQUA) [55]. The novelty of this approach lies in dividing the problem into two sub-parts: determining the *tilt* and *heading* quaternions. This separation ensures that magnetic disturbances do not affect the roll and pitch of the sensor's orientation. The authors demonstrate how to effectively fuse gyroscope, accelerometer, and magnetic readings into quaternion form. Analytically and empirically, the method proves its effectiveness by outperforming other common methods in tracking orientation relative to the Earth frame.

3.5.1 Symbols and Definitions

In Hamiltonian space a unit quaternion ${}^{\mathrm{A}}_{\mathrm{B}}q \in H^4$ also referred to as versor expresses the orientation of a frame A relative to B in 3D euclidean space:

$$ {}^{\mathrm{A}}_{\mathrm{B}}q = [q_w, q_x, q_y, q_z]^T = \left[\cos\frac{\alpha}{2}, e_x \sin\frac{\alpha}{2}, e_y \sin\frac{\alpha}{2}, e_z \sin\frac{\alpha}{2}\right]^T . $$

The unit vector $e = [e_x, e_y, e_z]^T$ and α represents the rotation axis and angle around the axis respectively (see Figure 3.10). The conjugate quaternion ${}^{\mathrm{A}}_{\mathrm{B}}q^* = {}^{\mathrm{B}}_{\mathrm{A}}q = [q_0, -q_1, -q_2, -q_3]$ expresses the orientation of a frame B relative to A. In other words, the conjugate is equivalent to inverse rotation of the frame A to B.

The quaternions are generally written in an algebraic form $q = q_0 + q_1 i + q_2 j + q_3 k$, where q_0, q_1, q_2 and q_3 are real numbers and i, j, k basis elements. The fundamental formula for quaternion multiplication $i^2 = j^2 = k^2 = ijk = -1$ relates the basis elements. The first component q_0 is usually referred to as the real or scalar part of q. The remaining part $q_1 i + q_2 j + q_3 k$ is called the imaginary or vector part of q. The muliplication is therefore

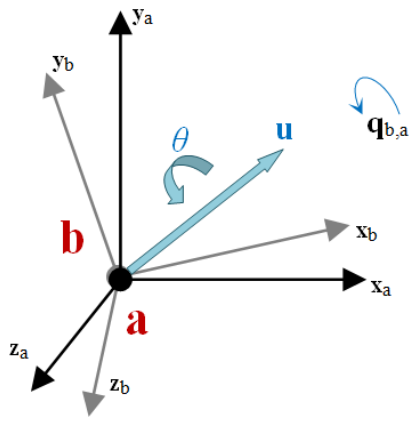

Figure 3.10: Geometric meaning of quaternion.

defined as:

$$qp = \begin{bmatrix} q_0p_0 - q_1p_1 - q_2p_2 - q_3p_3 \\ q_0p_1 + q_1p_0 + q_2p_3 - q_3p_2 \\ q_0p_2 - q_1p_3 + q_2p_0 + q_3p_1 \\ q_0p_3 + q_1p_2 - q_2p_1 + q_3p_0 \end{bmatrix}$$

Apart from applications in pure mathematics, the quarterions simplify calculations involving three-dimensional rotations. A pure quaternion (or vector quaternion) is a quaternion whose scalar part is equal to 0. This kind of quaternions appear often in 3D rotations. Let a vector ${}^{\mathrm{A}}v = [v_x, v_y, v_z]^T$ be expressed with respect to frame A. To obtain the same vector with respect to frame B, the vector ${}^{\mathrm{A}}v$ is rewritten as a pure quaternion ${}^{\mathrm{A}}v_q = [0, v_x, v_y, v_z]$, and muliplied with the versor ${}^{\mathrm{A}}_{\mathrm{B}}q$ and its conjugate ${}^{\mathrm{A}}_{\mathrm{B}}q^*$:

$${}^{\mathrm{B}}v_q = {}^{\mathrm{B}}_{\mathrm{A}}q \, {}^{\mathrm{A}}v_q \, {}^{\mathrm{A}}_{\mathrm{B}}q^*$$

Quaternion and Direct Cosine Matrix (DCM)

Interpreting a unit quaternion ${}^{A}_{B}q$ as the orientation implies that the corresponding DCM must exist. The matrix per definition belongs to orthogonal matrixes and describes the rotation in 3D euclidean space:

$$R\left({}^{A}_{B}q\right) = \begin{bmatrix} (q_0^2 + q_1^2 - q_2^2 - q_3^2) & 2(q_1q_2 + q_0q_3) & 2(q_1q_3 - q_0q_2) \\ 2(q_1q_2 - q_0q_3) & (q_0^2 - q_1^2 + q_2^2 - q_3^2) & 2(q_2q_3 + q_0q_1) \\ 2(q_1q_3 + q_0q_2) & 2(q_2q_3 - q_0q_1) & (q_0^2 - q_1^2 - q_2^2 + q_3^2) \end{bmatrix}$$

There are a variety of ways to convert the DCM to quaternion where only one is numerically stable. In literature the method is described in detail and proved the stability of the calculations.

Interpolations

The orientation tracking algorithms using IMU produce normally two estimations for the orientation of the technical frame. Quaternion-based algorithms fuse the estimates using either a linear (LERP) or spherical linear interpolation (SLERP) (see Figure 3.11).

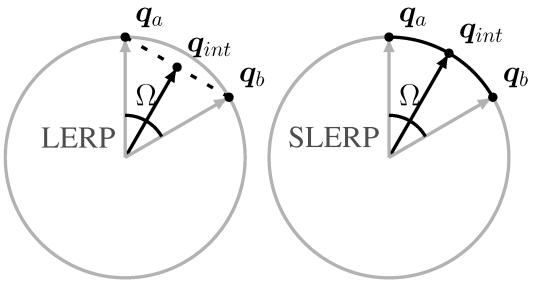

Figure 3.11: LERP and SLERP interpolations.

The LERP between two quaternions q and p is calculated as:

$$\overline{r} = (1-\alpha)p + \alpha q,\ \hat{r} = \frac{\overline{r}}{||\overline{r}||}$$

where $\alpha \in [0, 1]$. The SLERP in contrast evaluates the weighted average of two quaternions lying on the surface of 4D hypersphere:

$$\hat{r} = \frac{\sin\left((1-\alpha)\Omega\right)}{\sin\Omega}p + \frac{\sin\left(\alpha\Omega\right)}{\sin\Omega}q.$$

3.5.2 Algorithm

The quaternion-based algorithm leverages a complementary filter to fuse the orientation estimation from the gyroscope with delta quaternions of the accelerometer and magnetometer (see Figure 3.12). The orientation from gyroscope data goes through high-pass filtering due to low-frequency noise. In the same way, the orientation from accelerometer and magnetometer passes through low-pass filtering affected by high-frequency noise. Ideally, the fusion delivers a drift- and noise-free all-pass estimate of the orientation.

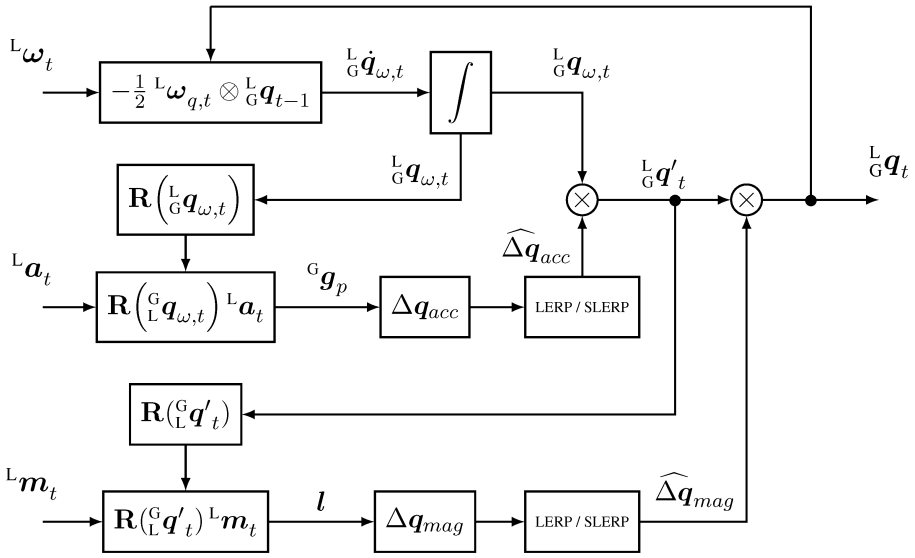

Figure 3.12: Complementary filter design.

Each iteration k of the algorithm consists of *prediction* and *correction* steps.

In the first step, the initial estimate of the orientation is derived from the measured angular velocity. The angular velocity ${}^{L}w = [w_x, w_y, w_z]^T$ may not be normalized and must be expressed in *radians per second*. To estimate the orientation of the Earth frame in respect to technical frame, the quaternion derivative is numerically integrated with the sampling period $\Delta t = t_k - t_{k-1}$:

$$ {}^{L}_{G}q_{w,t_k} = {}^{L}_{G}q_{t_{k-1}} + {}^{L}_{G}\dot{q}_{w,t_k}\Delta t. $$

The previous estimate ${}^{L}_{G}q_{t_{k-1}}$ is assumed to be known. The quaternion derivative ${}^{L}_{G}\dot{q}_{w,t_k}$ is computed using the following identity:

$$ {}^{L}_{G}\dot{q}_{w,t_k} = \frac{1}{2}\, {}^{L}_{G}q_{t_{k-1}}\, {}^{L}w_{q,t_k}, $$

where ${}^{L}w_{q,t_k}$ is the angular velocity expressed via pure quaternion.

The correction step utilizes accelerometer and magnetometer data to enhance the orientation. The gravity vector adjusts the frame's roll and pitch, while a yaw angle correction is derived from the magnetic North. The readings from the accelerometer and magnetometer are independently denoised using a first-order low-pass filter. The final estimation is

computed using the following expression with two delta quaternions:

$$^{L}_{G}q = {}^{L}_{G}q_w \Delta q_{\text{acc}} \Delta q_{\text{mag}}.$$

The authors in [55] derive correction terms solving in deterministic way the Wahba's Problem [57]. Without going into details, the accelerometer correction term is equal to

$$\Delta q_{ACC} = \left[\sqrt{\frac{G_z + 1}{2}}, -\frac{G_y}{\sqrt{2(G_z + 1)}}, \frac{G_x}{\sqrt{2(G_z + 1)}}, 0 \right]^T,$$

and the magnetometer one is

$$\Delta q_{ACC} = \left[\sqrt{\frac{G_z + 1}{2}}, -\frac{G_y}{\sqrt{2(G_z + 1)}}, \frac{G_x}{\sqrt{2(G_z + 1)}}, 0 \right]^T,$$

Both terms are subjected to high frequency noise, so the delta quaternions are scaled down by using LERP or SLERP with the identity quternion $q_I = [1, 0, 0, 0]^T$:

$$\overline{\Delta q_{\text{ACC}}} = (1 - \alpha) q_I + \alpha \Delta q_{\text{ACC}}$$

This kind of interpolation acts here as a first-order low-pass filter with the gain α characterizing the cut-off frequency of the filter.

The initial orientation is estimated from the first available acceleration and magnetic field vectors. Hence, the filter's initialization is performed in one single step:

$$^{L}_{G}q_0 = q_{\text{acc}} q_{\text{mag}}.$$

3.6 Joint Angle Measurement

by Nataliya Didukh

For the joint angle measurement, we assume that j_1 and j_2 are determined using the algorithm described in Section 3.4. Additionally, the orientation of sensors to the common reference coordinate system is known and described via rotation matrices $R_1(t)$ and $R_2(t)$. In this work, the common reference coordinate system is established through sensor fusion (accelerometer, gyroscope, and magnetometer). According to the definition, j_1

and j_2 must satisfy the equation $R_1(t)j_1 = R_2(t)j_2$, $\forall t$. Following this, the angle can be estimated as:

$$\alpha_m(t) = \sphericalangle_{3d}\left(R_1(t)(j_1 \times c), R_2(t)(j_2 \times c)\right), \tag{3.9}$$

where c is an arbitrary vector that is not co-linear with j_1 and j_2. The estimated angle is linearly proportional to a joint angle with a bias $\alpha_j = \alpha_m + \alpha_b$. The exact value of α_b has to be determined based on a zero pose (the pose at which the joint angle is known).

4 Results

The chapter presents the key results obtained from the assessment of the angle measurement algorithm using the algorithm introduced in Chapter 3. Initially, the demographic data of the participants is presented to demonstrate the representativeness of the algorithm's performance across different individuals. Subsequently, each subject underwent a series of prescribed exercises with specified repetitions, following a protocol designed to evaluate the algorithmś performance within individuals. Furthermore, each participant was equipped with sensors arranged in one of three configurations to assess the algorithm's performance under various sensor placement scenarios. Ultimately, the chapter presents the descriptive statistics of Root Mean Square Error (RMSE) in comparison to the ground truth, organized by participant, exercise, and the configuration of sensor placement.

4.1 Knee Axis

by Ihor Zhvanko

In this section, the effectiveness of the particle filter in tracking the knee axis is demonstrated via user-friendly interpretation. Figures 4.1,4.2,4.3 highlight instances of reliable tracking to contribute to the overall support the hypothesis that the method can reliably track the knee axis in real-time during dynamic exercises. Even through this section does not present any specific metrics, this illustration aims to intuitively convey the essence of knee axis tracking.

Each plot depicts the particle filter's tracking of the knee axis during various exercises. Notably, the different level of stability can particularly be observed during low- and high-intensity exercises. More precise variations are further outlined in the tabular data below manifesting this observation.

Table 4.1 presents the standard deviations of knee axis coordinates (X, Y, Z) over a series of exercise repetitions for each subject to demonstrate the reliability of real-time

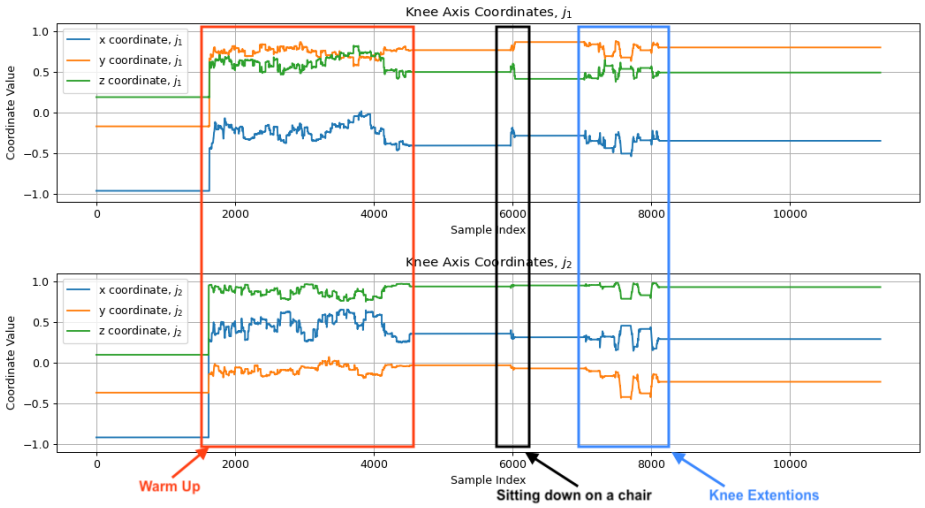

Figure 4.1: Knee axis tracking in coordinate frames of two sensors during knee extensions.

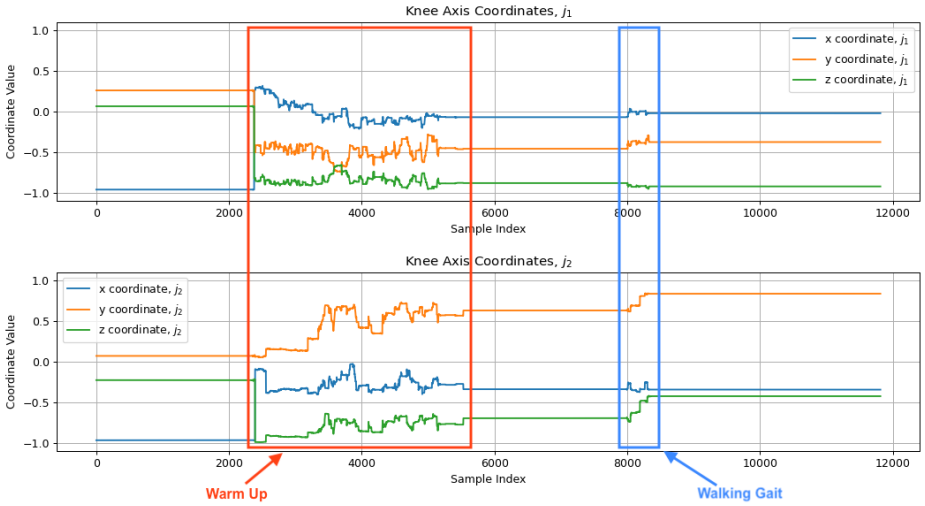

Figure 4.2: Knee axis tracking in coordinate frames of two sensors during walking gait.

axis tracking. These findings contribute to a broader understanding of the effectiveness of angle measurement by revealing varying levels of stability along coordinate axes.

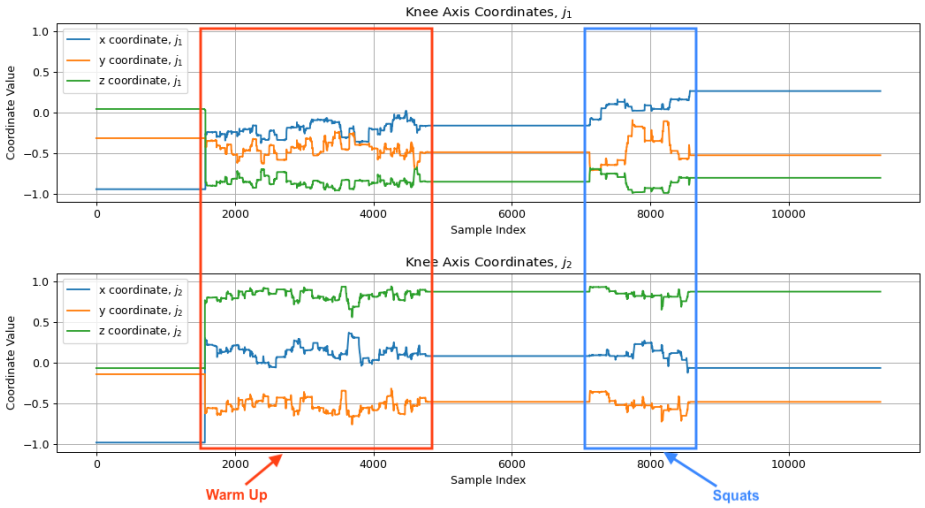

Figure 4.3: Knee axis tracking in coordinate frames of two sensors during squats.

Subject	Exercise		
	Walking	**Squatting**	**Knee Extensions**
001	0.12	0.35	0.23
002	0.11	0.33	0.19
003	0.09	0.27	0.23
004	0.11	0.27	0.28

Table 4.1: Variation of Knee Axis by Subject and Exercise.

4.2 Knee Angle

by Nataliya Didukh, Ihor Zhvanko

This section presents the Root Mean Square Error (RMSE) between the knee extension/flexion angle obtained through the ART system and two IMU devices. The descriptive statistics of RMSE over participants, exercises and sensor placement is included as well. The focus lies on examining the RMSE to assess the accuracy and reliability of the IMU-based measurements across different exercises, participants and sensor placement. In addition, Figures 4.4,4.5,4.6 demonstrate examples of knee angle tracking, visually assessing the performance of the IMU sensors in capturing knee movement dynamics during specific exercises.

Instances of knee angle tracking

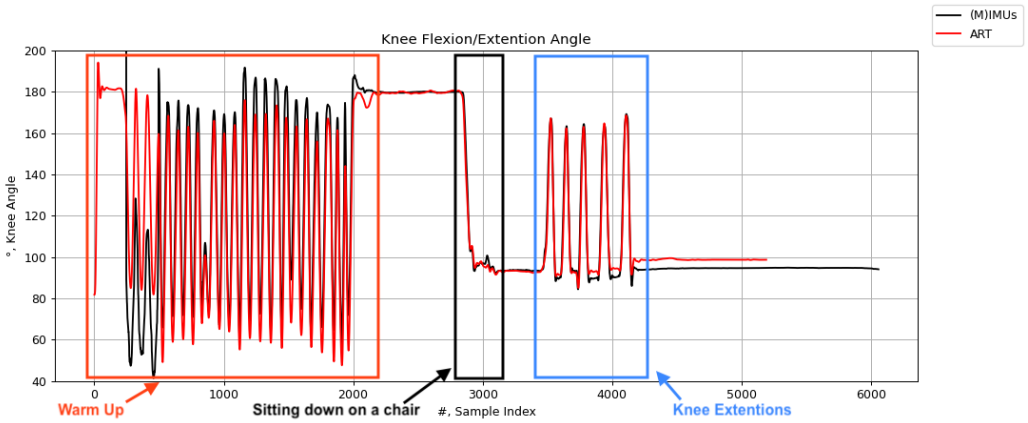

Figure 4.4: Knee angle during knee extensions.

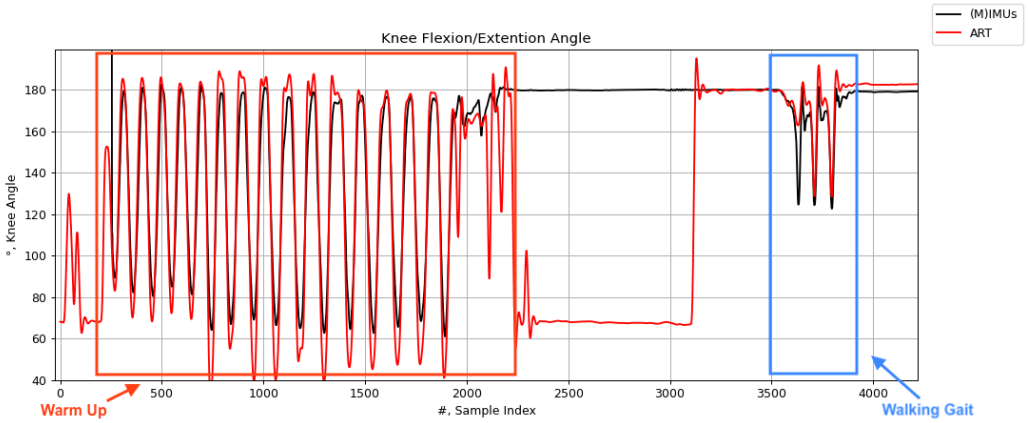

Figure 4.5: Knee angle during walking gait.

RMSE by each exercise and participant over sensor placements

Table 1 displays the RMSE values for each participant and exercise, illustrating the accuracy of the IMU sensor-based knee angle measurements in comparison to the ground truth obtained from the ART optical capture system.

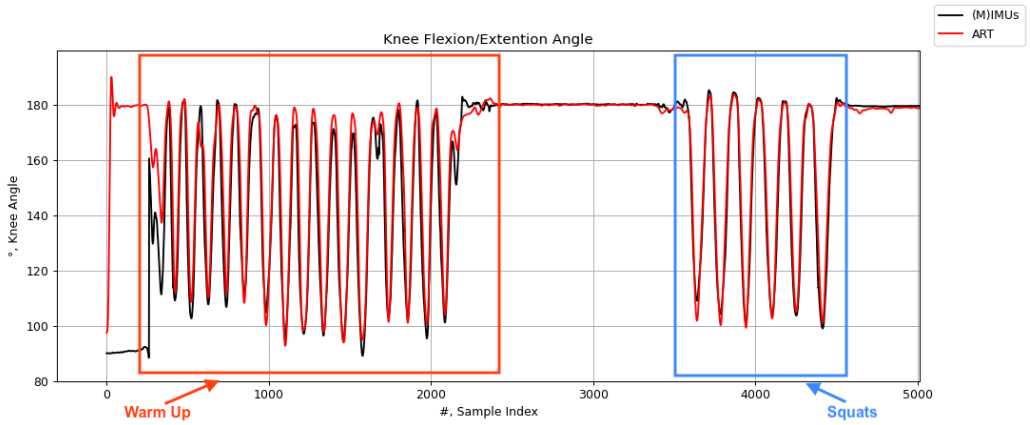

Figure 4.6: Knee angle during squats.

Exercise/Participant	001	002	003	Mean	Std
Walking Gait	2.34	2.89	2.12	2.45	0.472
Squatting	4.76	4.05	3.98	4.2625	0.427
Knee Extensions	2.10	2.15	1.87	2.04	0.128

Table 4.2: RMSE values for each participant and exercise.

RMSE by each exercise and sensor placement over participants

Examining the variations in RMSE based on different sensor placements, Table 3 highlights the performance differences observed between upper and lower leg sensor locations across all exercises and participants.

Exercise/Configuration	001	002	003	Mean	Std
Walking Gait	2.41	2.10	2.84	2.45	0.372
Squatting	4.23	4.16	4.4	4.26	0.107
Knee Extensions	1.99	1.83	2.3	2.04	0.235

Table 4.3: RMSE values for each sensor placement configuration and exercise.

Collectively, these tables offer a comprehensive overview of the accuracy and consistency of knee angle measurements derived from IMU sensors across various exercises and participants. This facilitates a nuanced understanding of the sensor's performance in the context of this study.

5 Discussion

Contributions

by Nataliya Didukh

The primary goal of this research was to devise a robust calibration method for knee axis tracking using Particle Filter methods, assessing the resulting algorithm's accuracy and repeatability in measuring knee joint angles. The introduced kinematic constraints, differing from those in previous literature, played a pivotal role. Specifically, constraints incorporating angular velocity measured by gyroscopes in the coordinate frame of the first sensor were employed, with transformations facilitated by the relative orientation of sensors. The algorithm's real-time capabilities and adaptability to soft-tissue artifacts and sensor displacements further distinguish it, contributing to the creation of a fast, adaptive, and noise-resistant knee joint extension angle measurement tool.

Upon assessing the method across four participants, three mounting points, and five exercises, the results demonstrated remarkable accuracy, with about a 4° RMSE compared to optical capture as ground truth. Interestingly, the algorithm displayed stability across different sensor placements, indicating its agnosticism to varied configurations. The observed correlation between exercise intensity and angle measurement precision highlights the algorithm's sensitivity to dynamic conditions. Visual confirmation through Figures 4.4, 4.5, 4.6 and further supports the algorithm's consistency with optical capture, while Figures 4.1, 4.2, 4.3 exposes knee axis fluctuations, potentially attributed to soft-tissue artifacts.

This study extends beyond previous research by examining dynamic exercises, introducing a real-time knee axis tracking algorithm for adaptability to perturbations. In contrast to earlier works focusing on walking gait [50], our exploration of diverse conditions, including three sensor placements and five exercises, adds valuable insights. The methodology raises the bar by addressing challenges posed by muscle exposure and uncertainties in dynamic environments.

Limitations, Implications, and Future Research

by Nataliya Didukh, Ihor Zhvanko

The challenges encountered in developing a particle filter for a static system, formulating a suitable knee joint constraint, and operating without active optical markers underscore the complexity of the research. Notably, the absence of input and reliance on noise to model uncertainties posed a unique challenge. The limitations, such as the requirement for a warm-up period and the use of passive optical markers, acknowledge areas for improvement. Future work should address these challenges to enhance the methodology's robustness and comparability with existing research.

The algorithm's potential application in recognizing and monitoring the Range of Motion (RoM) in knee rotations offers practical implications for everyday life and sports activities. Furthermore, the methodology provides a foundation for developing algorithms for different joints or constraints. Future research should explore ways to eliminate relative orientation in constraint equations, optimize particle numbers, and evaluate performance using established ground truth markers.

Bibliography

[1] A., Brand R.: Can Biomechanics Contribute to Clinical Orthopaedic Assessments? In: *The Iowa Orthopaedic Journal* 9 (1989), S. 61–64

[2] Arulampalam, M.S. ; Maskell, S. ; Gordon, N. ; Clapp, T.: A tutorial on particle filters for online nonlinear/non-Gaussian Bayesian tracking. In: *IEEE Transactions on Signal Processing* 50 (2002), Nr. 2, S. 174–188

[3] Bachmann, Eric R.: *Inertial and Magnetic Tracking of Limb Segment Orientation for Inserting Humans into Synthetic Environments*, NAVAL POSTGRADUATE SCHOOL MONTEREY CA, Dissertation, dec 2000

[4] Baker, Richard: Gait analysis methods in rehabilitation. In: *J Neuroeng Rehabil* 3 (2006), März, S. 4

[5] Bulling, Andreas ; Blanke, Ulf ; Schiele, Bernt: A Tutorial on Human Activity Recognition Using Body-Worn Inertial Sensors. In: *ACM Comput. Surv.* 46 (2014), jan, Nr. 3. – URL https://doi.org/10.1145/2499621. – ISSN 0360-0300

[6] Cappozzo, Aurelio ; Della Croce, Ugo ; Leardini, Alberto ; Chiari, Lorenzo: Human movement analysis using stereophotogrammetry. Part 1: theoretical background. In: *Gait Posture* 21 (2005), Februar, Nr. 2, S. 186–196

[7] Chen, Yawen ; Fu, Chenglong ; Leung, Winnie Suk W. ; Shi, Ling: Drift-Free and Self-Aligned IMU-Based Human Gait Tracking System With Augmented Precision and Robustness. In: *IEEE Robotics and Automation Letters* 5 (2020), Nr. 3, S. 4671–4678

[8] Cheng, Peng ; Oelmann, Bengt: Joint-Angle Measurement Using Accelerometers and Gyroscopes—A Survey. In: *IEEE Transactions on Instrumentation and Measurement* 59 (2010), Nr. 2, S. 404–414

[9] Cooper, Glen ; Sheret, Ian ; McMillan, Louise ; Siliverdis, Konstantinos ; Sha, Ning ; Hodgins, Diana ; Kenney, Laurence ; Howard, David: Inertial sensor-based knee flexion/extension angle estimation. In: *J Biomech* 42 (2009), September, Nr. 16, S. 2678–2685

[10] Cordillet, Sébastien ; Bideau, Nicolas ; Bideau, Benoit ; Nicolas, Guillaume: Estimation of 3D Knee Joint Angles during Cycling Using Inertial Sensors: Accuracy of a Novel Sensor-to-Segment Calibration Procedure Based on Pedaling Motion. In: *Sensors (Basel)* 19 (2019), Mai, Nr. 11

[11] Cutti, Andrea G. ; Ferrari, Alberto ; Garofalo, Pietro ; Raggi, Michele ; Cappello, Angelo ; Ferrari, Adriano: 'Outwalk': a protocol for clinical gait analysis based on inertial and magnetic sensors. In: *Med Biol Eng Comput* 48 (2009), November, Nr. 1, S. 17–25

[12] Dejnabadi, H. ; Jolles, B.M. ; Aminian, K.: A new approach to accurate measurement of uniaxial joint angles based on a combination of accelerometers and gyroscopes. In: *IEEE Transactions on Biomedical Engineering* 52 (2005), Nr. 8, S. 1478–1484

[13] Dejnabadi, Hooman ; Jolles, Brigitte M. ; Casanova, Emilio ; Fua, Pascal ; Aminian, Kamiar: Estimation and visualization of sagittal kinematics of lower limbs orientation using body-fixed sensors. In: *IEEE Trans Biomed Eng* 53 (2006), Juli, Nr. 7, S. 1385–1393

[14] Ding, Ye ; Panizzolo, Fausto A. ; Siviy, Christopher ; Malcolm, Philippe ; Galiana, Ignacio ; Holt, Kenneth G. ; Walsh, Conor J.: Effect of timing of hip extension assistance during loaded walking with a soft exosuit. In: *J Neuroeng Rehabil* 13 (2016), Oktober, Nr. 1, S. 87

[15] Doucet, Arnaud ; Godsill, Simon ; Andrieu, Christophe: On sequential Monte Carlo sampling methods for Bayesian filtering. In: *Statistics and Computing* 10 (2000), Juli, Nr. 3, S. 197–208

[16] Ehrig, Rainald M. ; Taylor, William R. ; Duda, Georg N. ; Heller, Markus O.: A survey of formal methods for determining the centre of rotation of ball joints. In: *Journal of Biomechanics* 39 (2006), Nr. 15, S. 2798–2809. – ISSN 0021-9290

[17] Elfring, Jos ; Torta, Elena ; Molengraft, René van de: Particle Filters: A Hands-On Tutorial. In: *Sensors (Basel)* 21 (2021), Januar, Nr. 2

[18] Fan, Bingfei ; Li, Qingguo ; Tan, Tian ; Kang, Peiqi ; Shull, Peter B.: Effects of IMU Sensor-to-Segment Misalignment and Orientation Error on 3-D Knee Joint Angle Estimation. In: *IEEE Sensors Journal* 22 (2022), Nr. 3, S. 2543–2552

[19] Fasel, Benedikt ; Spörri, Jörg ; Schütz, Pascal ; Lorenzetti, Silvio ; Aminian, Kamiar: Validation of functional calibration and strap-down joint drift correction for computing 3D joint angles of knee, hip, and trunk in alpine skiing. In: *PLoS One* 12 (2017), Juli, Nr. 7, S. e0181446

[20] Favre, J ; Jolles, B M. ; Aissaoui, R ; Aminian, K: Ambulatory measurement of 3D knee joint angle. In: *J Biomech* 41 (2008), Januar, Nr. 5, S. 1029–1035

[21] Ferrari, Alberto ; Cutti, Andrea G. ; Garofalo, Pietro ; Raggi, Michele ; Heijboer, Monique ; Cappello, Angelo ; Davalli, Angelo: First in vivo assessment of "Outwalk": a novel protocol for clinical gait analysis based on inertial and magnetic sensors. In: *Med Biol Eng Comput* 48 (2009), November, Nr. 1, S. 1–15

[22] Gabiccini, Marco ; Stillfried, Georg ; Marino, Hamal ; Bianchi, Matteo: A data-driven kinematic model of the human hand with soft-tissue artifact compensation mechanism for grasp synergy analysis. In: *2013 IEEE/RSJ International Conference on Intelligent Robots and Systems*, 2013, S. 3738–3745

[23] Galperin, Irina ; Hillel, Inbar ; Del Din, Silvia ; Bekkers, Esther M J. ; Nieuwboer, Alice ; Abbruzzese, Giovanni ; Avanzino, Laura ; Nieuwhof, Freek ; Bloem, Bastiaan R. ; Rochester, Lynn ; Della Croce, Ugo ; Cereatti, Andrea ; Giladi, Nir ; Mirelman, Anat ; Hausdorff, Jeffrey M.: Associations between daily-living physical activity and laboratory-based assessments of motor severity in patients with falls and Parkinson's disease. In: *Parkinsonism Relat Disord* 62 (2019), Januar, S. 85–90

[24] Grood, E S. ; Suntay, W J.: A joint coordinate system for the clinical description of three-dimensional motions: application to the knee. In: *J Biomech Eng* 105 (1983), Mai, Nr. 2, S. 136–144

[25] Habtemariam, Biruk K. ; Tharmarasa, R. ; Kirubarajan, T.: PHD filter based track-before-detect for MIMO radars. In: *Signal Processing* 92 (2012), Nr. 3, S. 667–678. – URL https://www.sciencedirect.com/science/article/pii/S0165168411003070. – ISSN 0165-1684

[26] Inc, MBIENTLAB: *METAMOTIONS*. 2023. – URL http://web.archive.org/web/20230726011407/https://mbientlab.com/metamotions. – Zugriffsdatum: 2023-07-26

[27] Kim, Sung-Kyun ; Hong, Seokmin ; Kim, Doik: A walking motion imitation framework of a humanoid robot by human walking recognition from IMU motion data. In: *2009 9th IEEE-RAS International Conference on Humanoid Robots*, 2009, S. 343–348

[28] Laidig, Daniel ; Müller, Philipp ; Seel, Thomas: Automatic anatomical calibration for IMU-based elbow angle measurement in disturbed magnetic fields. In: *Current Directions in Biomedical Engineering* 3 (2017), Nr. 2, S. 167–170. – URL https://doi.org/10.1515/cdbme-2017-0035

[29] Lee, Jung K. ; Jeon, Tae H.: IMU-Based but Magnetometer-Free Joint Angle Estimation of Constrained Links. In: *2018 IEEE SENSORS*, 2018, S. 1–4

[30] Lee, Jung K. ; Jeon, Tae H.: Magnetic Condition-Independent 3D Joint Angle Estimation Using Inertial Sensors and Kinematic Constraints. In: *Sensors* 19 (2019), Nr. 24. – URL https://www.mdpi.com/1424-8220/19/24/5522. – ISSN 1424-8220

[31] Lee, Jung K. ; Jeon, Tae H. ; Jung, Woo C.: Constraint-augmented Kalman Filter for Magnetometer-free 3D Joint Angle Determination. In: *International Journal of Control, Automation and Systems* 18 (2020), November, Nr. 11, S. 2929–2942

[32] Lee, Jung K. ; Park, Edward J.: Minimum-Order Kalman Filter With Vector Selector for Accurate Estimation of Human Body Orientation. In: *IEEE Transactions on Robotics* 25 (2009), Nr. 5, S. 1196–1201

[33] Li, Tiancheng ; Bolic, Miodrag ; Djuric, Petar M.: Resampling Methods for Particle Filtering: Classification, implementation, and strategies. In: *IEEE Signal Processing Magazine* 32 (2015), Nr. 3, S. 70–86

[34] Li, Tiancheng ; Sattar, Tariq P. ; Han, Qing ; Sun, Shudong: Roughening methods to prevent sample impoverishment in the particle PHD filter. In: *Proceedings of the 16th International Conference on Information Fusion*, 2013, S. 17–22

[35] Lin, Pei-Chun ; Ho, Chi-Wei: Design and implementation of a 9-axis inertial measurement unit. In: *2009 IEEE International Conference on Robotics and Automation*, 2009, S. 736–741

[36] Liu, Jun S. ; Chen, Rong: Sequential Monte Carlo Methods for Dynamic Systems. In: *Journal of the American Statistical Association* 93 (1998), Nr. 443, S. 1032–1044. – URL http://www.jstor.org/stable/2669847. – Zugriffsdatum: 2023-05-17. – ISSN 01621459

[37] Mayagoitia, Ruth E. ; Nene, Anand V. ; Veltink, Peter H.: Accelerometer and rate gyroscope measurement of kinematics: an inexpensive alternative to optical motion analysis systems. In: *J Biomech* 35 (2002), April, Nr. 4, S. 537–542

[38] Musso, C. ; Oudjane, Nadia ; Gland, François: Improving regularized particle filters. (2001), 01

[39] Müller, Philipp ; Bégin, Marc-André ; Schauer, Thomas ; Seel, Thomas: Alignment-Free, Self-Calibrating Elbow Angles Measurement Using Inertial Sensors. In: *IEEE Journal of Biomedical and Health Informatics* 21 (2017), Nr. 2, S. 312–319

[40] Nagymáté, Gergely ; Kiss, Rita M.: Affordable gait analysis using augmented reality markers. In: *PLoS One* 14 (2019), Februar, Nr. 2, S. e0212319

[41] Niswander, Wesley ; Wang, Wei ; Kontson, Kimberly: Optimization of IMU Sensor Placement for the Measurement of Lower Limb Joint Kinematics. In: *Sensors* 20 (2020), Nr. 21. – URL https://www.mdpi.com/1424-8220/20/21/5993. – ISSN 1424-8220

[42] Noury, N ; Fleury, A ; Rumeau, P ; Bourke, A K. ; Laighin, G O. ; Rialle, V ; Lundy, J E.: Fall detection–principles and methods. In: *Annu Int Conf IEEE Eng Med Biol Soc* 2007 (2007), S. 1663–1666

[43] Ohtaki, Yasuaki ; Sagawa, Koichi ; Inooka, Hikaru: A Method for Gait Analysis in A Daily Living Environment Using Body-mounted Instruments. In: *JSME International Journal Series C* 44 (2001), 12, S. 1125–1132

[44] Osder, Stephen ; Rouse, W. E. ; Young, L. S.: Navigation, guidance, and control systems for V/STOL aircraft., URL https://api.semanticscholar.org/CorpusID:108004765, 1973

[45] O'Donovan, Karol J. ; Kamnik, Roman ; O'Keeffe, Derek T. ; Lyons, Gerard M.: An inertial and magnetic sensor based technique for joint angle measurement. In: *Journal of Biomechanics* 40 (2007), Nr. 12, S. 2604–2611. – URL https://www.sciencedirect.com/science/article/pii/S0021929007000103. – ISSN 0021-9290

[46] Pacher, Léonie ; Chatellier, Christian ; Vauzelle, Rodolphe ; Fradet, Laetitia: Sensor-to-Segment Calibration Methodologies for Lower-Body Kinematic Analysis with Inertial Sensors: A Systematic Review. In: *Sensors* 20 (2020), Nr. 11. – URL https://www.mdpi.com/1424-8220/20/11/3322. – ISSN 1424-8220

[47] Palermo, Eduardo ; Rossi, Stefano ; Marini, Francesca ; Patanè, Fabrizio ; Cappa, Paolo: Experimental evaluation of accuracy and repeatability of a novel body-to-sensor calibration procedure for inertial sensor-based gait analysis. In: *Measurement* 52 (2014), S. 145–155. – URL https://www.sciencedirect.com/science/article/pii/S0263224114000980. – ISSN 0263-2241

[48] Picerno, Pietro: 25 years of lower limb joint kinematics by using inertial and magnetic sensors: A review of methodological approaches. In: *Gait Posture* 51 (2016), November, S. 239–246

[49] Picerno, Pietro ; Cereatti, Andrea ; Cappozzo, Aurelio: Joint kinematics estimate using wearable inertial and magnetic sensing modules. In: *Gait Posture* 28 (2008), Mai, Nr. 4, S. 588–595

[50] Seel, Thomas ; Raisch, Jörg ; Schauer, Thomas: IMU-Based Joint Angle Measurement for Gait Analysis. In: *Sensors* 14 (2014), Nr. 4, S. 6891–6909. – URL https://www.mdpi.com/1424-8220/14/4/6891. – ISSN 1424-8220

[51] Seel, Thomas ; Schauer, Thomas ; Raisch, Jörg: Joint axis and position estimation from inertial measurement data by exploiting kinematic constraints. In: *2012 IEEE International Conference on Control Applications*, 2012, S. 45–49

[52] Tamburini, Paola ; Storm, Fabio ; Buckley, Chris ; Bisi, Maria C. ; Stagni, Rita ; Mazzà, Claudia: Moving from laboratory to real life conditions: Influence on the assessment of variability and stability of gait. In: *Gait Posture* 59 (2017), Oktober, S. 248–252

[53] Tham, Lai K. ; Osman, Noor Azuan A. ; Kouzbary, Mouaz A. ; Aminian, Kamiar: Biomechanical Ambulatory Assessment of 3D Knee Angle Using Novel Inertial Sensor-Based Technique. In: *IEEE Access* 9 (2021), S. 36559–36570

[54] Turgut, Begumhan ; Martin, Richard P.: Restarting Particle Filters: An Approach to Improve the Performance of Dynamic Indoor Localization. In: *GLOBECOM 2009 - 2009 IEEE Global Telecommunications Conference*, 2009, S. 1–7

[55] Valenti, Roberto G. ; Dryanovski, Ivan ; Xiao, Jizhong: Keeping a Good Attitude: A Quaternion-Based Orientation Filter for IMUs and MARGs. In: *Sensors* 15 (2015), Nr. 8, S. 19302–19330. – URL https://www.mdpi.com/1424-8220/15/8/19302. – ISSN 1424-8220

[56] Vargas-Valencia, L. S. ; Elias, A. ; Rocon, E. ; Bastos-Filho, T. ; Frizera, A.: An IMU-to-Body Alignment Method Applied to Human Gait Analysis. In: *Sensors (Basel)* 16 (2016), Dec, Nr. 12

[57] Wahba, Grace: A Least Squares Estimate of Satellite Attitude. In: *SIAM Review* 7 (1965), Nr. 3, S. 409–409. – URL https://doi.org/10.1137/1007077

[58] Willemsen, A T. ; Alsté, J A. van ; Boom, H B.: Real-time gait assessment utilizing a new way of accelerometry. In: *J Biomech* 23 (1990), Nr. 8, S. 859–863

[59] Willemsen, A.T.M. ; Frigo, C. ; Boom, H.B.K.: Lower extremity angle measurement with accelerometers-error and sensitivity analysis. In: *IEEE Transactions on Biomedical Engineering* 38 (1991), Nr. 12, S. 1186–1193

[60] Williamson, R ; Andrews, B J.: Detecting absolute human knee angle and angular velocity using accelerometers and rate gyroscopes. In: *Med Biol Eng Comput* 39 (2001), Mai, Nr. 3, S. 294–302

[61] Wong, Charence ; Zhang, Zhi-Qiang ; Lo, Benny ; Yang, Guang-Zhong: Wearable Sensing for Solid Biomechanics: A Review. In: *IEEE Sensors Journal* 15 (2015), Nr. 5, S. 2747–2760

[62] Wu, Ge ; Helm, Frans C T. van der ; Veeger, H E J D. ; Makhsous, Mohsen ; Van Roy, Peter ; Anglin, Carolyn ; Nagels, Jochem ; Karduna, Andrew R. ; McQuade, Kevin ; Wang, Xuguang ; Werner, Frederick W. ; Buchholz, Bryan ; International Society of Biomechanics: ISB recommendation on definitions

of joint coordinate systems of various joints for the reporting of human joint motion–Part II: shoulder, elbow, wrist and hand. In: *J Biomech* 38 (2005), Mai, Nr. 5, S. 981–992

[63] Wu, Ge ; Siegler, Sorin ; Allard, Paul ; Kirtley, Chris ; Leardini, Alberto ; Rosenbaum, Dieter ; Whittle, Mike ; D'Lima, Darryl D. ; Cristofolini, Luca ; Witte, Hartmut ; Schmid, Oskar ; Stokes, Ian ; Standardization and Terminology Committee of the International Society of Biomechanics: ISB recommendation on definitions of joint coordinate system of various joints for the reporting of human joint motion–part I: ankle, hip, and spine. International Society of Biomechanics. In: *J Biomech* 35 (2002), April, Nr. 4, S. 543–548

[64] Yi, Chunzhi ; Wei, Baichun ; Ding, Zhen ; Yang, Chifu ; Chen, Zhiyuan ; Jiang, Feng: A Self-Aligned Method of IMU-Based 3-DoF Lower-Limb Joint Angle Estimation. In: *IEEE Transactions on Instrumentation and Measurement* 71 (2022), S. 1–10

[65] Yin, Li ; Chen, Kaining ; Guo, Lin ; Cheng, Liangjun ; Wang, Fuyou ; Yang, Liu: Identifying the Functional Flexion-extension Axis of the Knee: An In-Vivo Kinematics Study. In: *PLoS One* 10 (2015), Juni, Nr. 6, S. e0128877

[66] Young, Alexander D.: Use of Body Model Constraints to Improve Accuracy of Inertial Motion Capture. In: *2010 International Conference on Body Sensor Networks*, 2010, S. 180–186

[67] Zabat, Mahdi ; Ababou, Amina ; Ababou, Noureddine ; Dumas, Raphaël: IMU-based sensor-to-segment multiple calibration for upper limb joint angle measurement-a proof of concept. In: *Med Biol Eng Comput* 57 (2019), August, Nr. 11, S. 2449–2460

[68] Zhang, Licong ; Sturm, Jürgen ; Cremers, Daniel ; Lee, Dongheui: Real-time human motion tracking using multiple depth cameras. In: *2012 IEEE/RSJ International Conference on Intelligent Robots and Systems*, 2012, S. 2389–2395

Erklärung zur selbstständigen Bearbeitung

Hiermit versichere ich, dass ich die vorliegende Arbeit ohne fremde Hilfe selbständig verfasst und nur die angegebenen Hilfsmittel benutzt habe. Wörtlich oder dem Sinn nach aus anderen Werken entnommene Stellen sind unter Angabe der Quellen kenntlich gemacht.

Ort	Datum	Unterschrift im Original

Erklärung zur selbstständigen Bearbeitung

Hiermit versichere ich, dass ich die vorliegende Arbeit ohne fremde Hilfe selbständig verfasst und nur die angegebenen Hilfsmittel benutzt habe. Wörtlich oder dem Sinn nach aus anderen Werken entnommene Stellen sind unter Angabe der Quellen kenntlich gemacht.

Ort	Datum	Unterschrift im Original